Journal of Sedimentary Research

Journal of Sedimentary Research, 2006, v. 76, 1304–1322
Research Article
DOI: 10.2110/jsr.2006.106

CHARACTERIZATION OF DOLOMITIZING FLUIDS IN THE CARBONIFEROUS OF THE CANTABRIAN ZONE (NW SPAIN): A FLUID-INCLUSION STUDY WITH CRYO-RAMAN SPECTROSCOPY

MARTA GASPARRINI,[1] RONALD J. BAKKER,[2] AND THILO BECHSTÄDT[1]
[1]*Geologisch-Paläontologisches Institut, Ruprecht-Karls-Universität Heidelberg, INF 234, D-69120 Heidelberg, Germany*
e-mail: bakker@unileoben.ac.at
[2]*Department of Applied Geosciences and Geophysics, Mineralogy & Petrology, University Leoben, Peter-Tunner-Strasse 5, A-8700, Leoben, Austria*

ABSTRACT: **A late diagenetic dolomitization pervasively affected Carboniferous carbonates of the Variscan Cantabrian Zone (NW Spain). The process generated replacive and void-filling dolomite phases, spatially related with various calcite cements. The nature of the diagenetic fluids has been investigated by cryo-Raman spectroscopy, i.e., a combination of Raman spectroscopy and low-temperature microthermometry, which reveals in great accuracy the salinity and the major types of dissolved cations and anions in single fluid inclusions. Fluid properties obtained only from microthermometry are distinctively different. The study demonstrates that this improved analytical method of fluid inclusions is a valuable contribution for the interpretation of fluids in dolomite research. In primary fluid inclusions of the Cantabrian dolomites, hydrohalite and two unknown salt hydrates, one of which resembles $MgCl_2 \cdot 12H_2O$, were detected by cryo-Raman spectroscopy, whereas only hydrohalite appeared in the calcite primary inclusions. The presence of $CaCl_2$ hydrates is suspected only from low eutectic temperatures. Dolomite formed from an evolving fluid, as reflected by the highly variable equivalent Na/Ca ratios calculated, at high and nearly constant total salinities. The approximately constant Na/Ca ratio in the first calcite cement reflects a homogeneous source for the salts. Cryo-Raman spectroscopy reveals that different cooling procedures may induce the formation of different phase assemblages within the same fluid inclusion in both dolomite and calcite. Consequently, fluid inclusions display different melting behaviors, corresponding to different values of calculated salinities. Salinity calculation only from microthermometry may lead to an underestimation of true salinities. According to an assumed hydrostatic geothermal gradient, maximum formation conditions for the dolomites are 150 ± 30°C and 40 ± 10 MPa, corresponding to a depth of 3.9 ± 1.0 km. The first calcite formed at 130 ± 20°C and 35 ± 5 MPa, corresponding to a depth of 3.4 ± 0.6 km. The minimum T–P of formation is defined by the homogenization conditions.**

INTRODUCTION

The uncertainties that surround the origin of dolomite have attracted the attention of Earth scientists for over two centuries. Nevertheless, the origin of massive dolomite is still a matter of debate (see reviews in Land 1985, Morrow 1990a, Morrow 1990b, and Machel 2005). Dolomitization models are, in general, based on geometry, local geology, cement petrography, fluid analyses, and hydrology aiming to understand why large dolomite bodies occur in limestones, how they form, and which is their three-dimensional distribution (the "dolomite problem;" see McKenzie 1991). One of the crucial questions focuses on the nature of the fluids, which can account for extensive dolomitization and their occurrence in diagenetic environments.

The main intensive properties (i.e., independent of mass, size, or shape of the carbonate rock) that determine dolomitization are temperature and composition of the fluid. Parameters of importance of the fluid composition are Mg/Ca ratio, salinity, CO_3/Ca ratio, and SO_4^{2-} concentration (e.g., Morrow 1990a; Usdowski 1994). In absence of remnants of this paleo-fluid, the properties of the dolomitizing fluid are mainly obtained indirectly by analyzing isotopic composition (strontium, oxygen, and carbon) of dolomite crystals. Fractionation of oxygen and carbon isotopes between dolomite crystals and the dolomitizing fluid also depends on temperature and composition, like dolomitization itself. Therefore, it is impossible to determine the initial fluid composition from oxygen and carbon isotopic composition of the dolomite alone (e.g., Wilson et al. 1990). In addition, a certain amount of uncertainty lies within fractionation factors, which are experimentally determined and may be greatly affected by the non-stoichiometry of dolomite and non-equilibrium conditions.

Fluid inclusions store information on temperature, pressure, and composition of the paleo-fluids. Therefore, fluid-inclusion studies may provide significant constraints on the thermal evolution and composition of ancient diagenetic fluids (e.g., Roedder 1984; Goldstein and Reynolds 1994). The use of fluid inclusions for a direct analysis of dolomitizing fluids became an approved method in the early 1990s (e.g., Coniglio et al. 1994; Wojcik et al. 1994), and it had a great impact on the interpretation of isotopic data. Most studies that have included fluid-inclusion data support a hydrothermal convection, due to high homogenization temperatures. This implies either high formation conditions or circulation of hot fluids in relatively "cold," shallow rocks. Based on microthermometric evidence, hydrothermal dolomites may form from a variety of fluids (e.g., Wilkinson 2003), ranging from low saline (seawater-like) to high saline (evaporitic brines). However, the analysis of fluid inclusions in dolomite and other carbonates is not a simple straightforward method. The size and the irregularity of individual inclusions and the lack of

 1527-1404/06/076-1304/$03.00

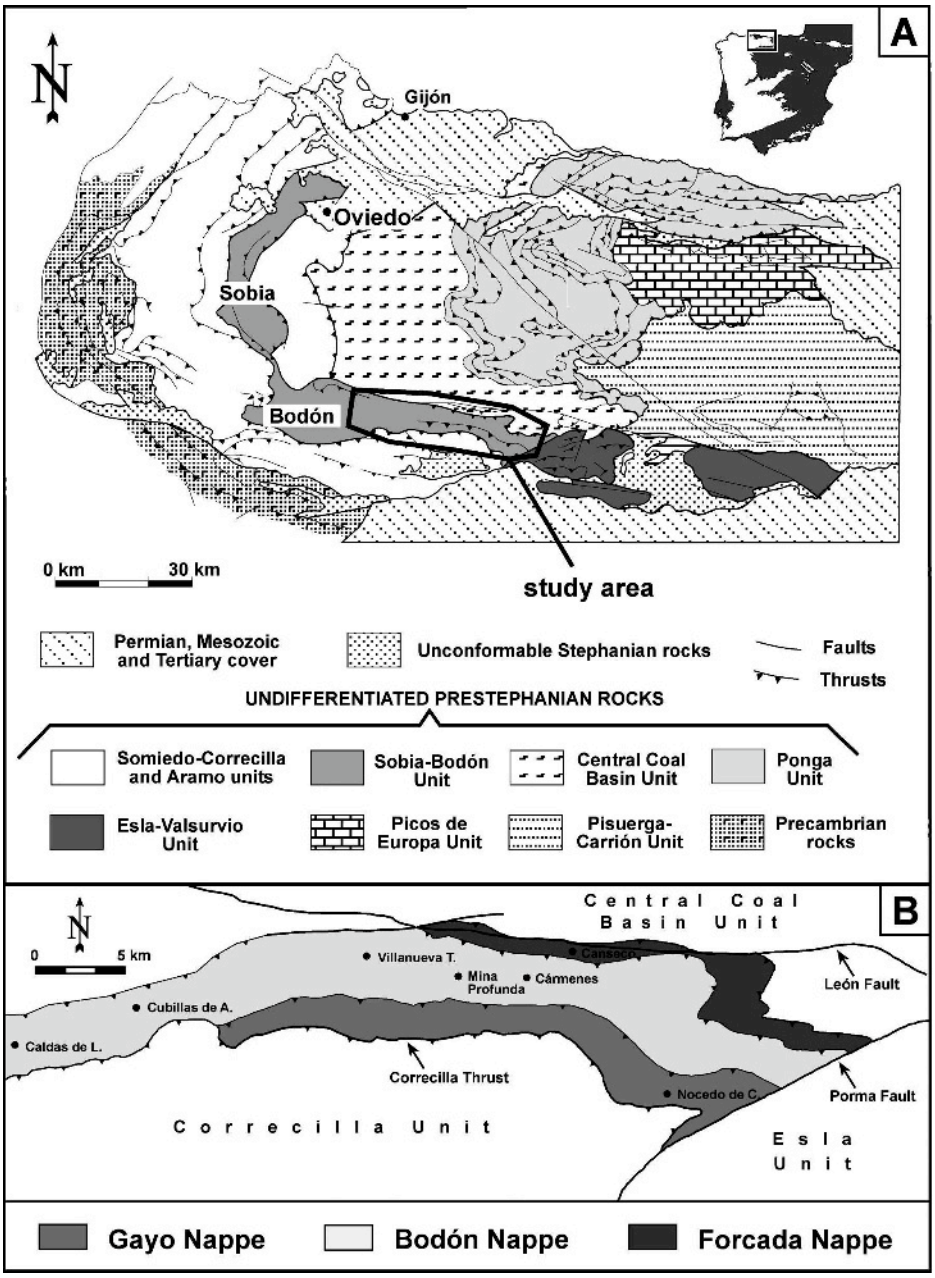

FIG. 1.—**A)** Geological sketch map of the Cantabrian Zone showing the different Variscan thrust units and the location of the study area (modified after Pérez-Estaún and Bastida 1990). **B)** Simplified tectonic sketch of the central and eastern Bodón Unit illustrating the location of the sampled sites (modified after Marcos 1968a). **C)** Schematic stratigraphic column of the studied area.

transparency of dolomite may prevent an accurate and reproducible microthermometrical analysis. Final melting temperatures of fluid inclusions are often missing or the phase that is finally melting is not specified, although these measurements are used to characterize the origin of fluids (e.g., evaporitic brine versus seawater). In addition, bulk solute data of aqueous fluid inclusions may reveal anion and cation contents (e.g., Banks and Yardley 1992) and can be used to constrain the origin of the fluid or water–rock interactions (like dolomitization and albitization). However, (1) carbonates are not suitable for this approach (Gleeson 2003), (2) the absolute concentration calculations depend on microthermometry (in the sense of equivalent mass% NaCl), and (3) the analyzed crystal should be dominated by one fluid generation.

In this study the cryo-Raman spectroscopy method, which combines Raman spectroscopy with low-temperature microthermometry (Bakker 2004), is applied to primary fluid inclusions in carbonates from an extensively dolomitized area. Our research illustrates the care with which these inclusions should be analyzed in order to obtain realistic results, and the benefits of using this combined analytical method, which could have a high impact on the interpretation of dolomitizing fluids overall. The study area is in the Cantabrian Zone (NW Spain), the Variscan foreland belt of the Iberian Peninsula, where a late diagenetic dolomitization pervasively affected various Paleozoic carbonates ranging in age from Early Cambrian to Late Carboniferous. Extensive dolomite bodies were reported from different areas of the Cantabrian Zone (e.g., Paniagua et al. 1996; Gómez-Fernández et al. 2000; Grimmer 2000; Tornos and Spiro 2000). Replacive and void-filling dolomites are found spatially related to distinct calcite cements. The origin of these mineral phases has been investigated by means of a multidisciplinary approach, which integrates fieldwork and microscopy observations with detailed fluid-inclusion research. The main goal of this study is to constrain the nature, temperature, and composition of the paleofluids, which originated the various mineral phases, and, thereby to constrain the origin of massive

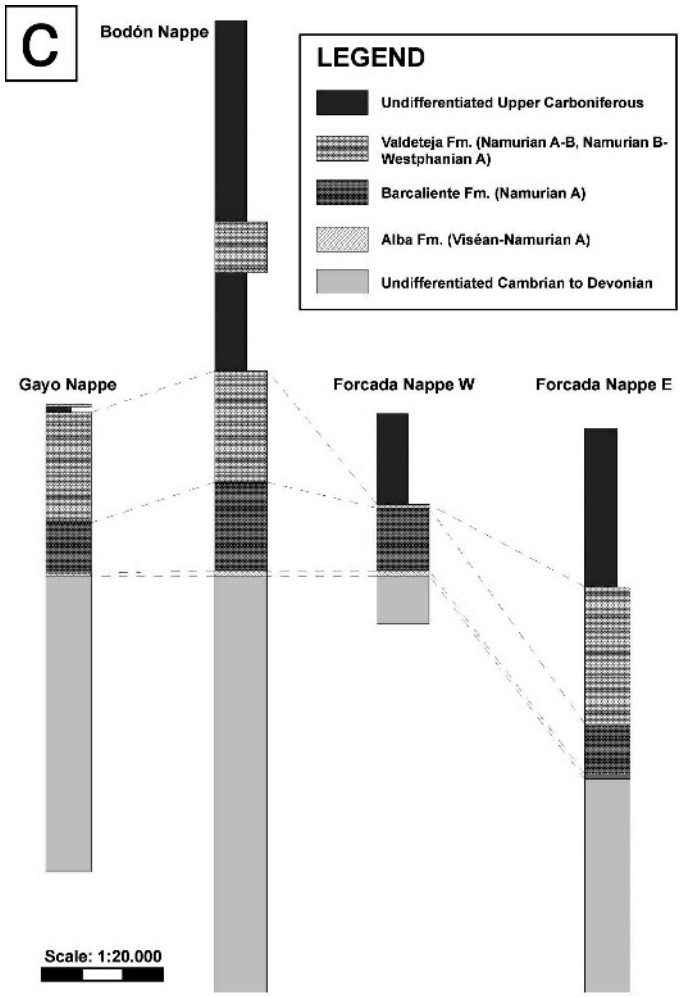

FIG. 1.—Continued.

dolomitization within the Carboniferous rock succession of the southwestern Cantabrian Zone.

Highly debatable is the low-temperature behavior of saline fluid inclusions (Bakker 2004). Fast cooling of saline fluid inclusions results in the formation of metastable ice-like phase assemblages that have a melting behavior different from that of the stable assemblage. The variable freezing behavior of the same inclusion, depending on cooling rates and temperature cycling procedures, indicates the care with which natural fluid inclusions should be treated to obtain true salinities. In this study, the salinity of fluid inclusions in dolomite and calcite is characterized by cryo-Raman spectroscopy. It is demonstrated that substantially more detail is gained from single fluid inclusions by this nondestructive method. Our research also illustrates that microthermometry, which is still a technique of major use for dolomitization studies, should be combined with Raman to obtain more accurate information about salinity and major salts of the fluids, this having the potential to contribute to improvements of dolomitization models.

GEOLOGICAL SETTING

The Cantabrian Zone in NW Spain represents the Variscan foreland thrust and fold belt of the Iberian Massif and consists of a Precambrian basement covered by Paleozoic sediments (e.g., Aramburu and Bastida 1995). This succession was thrusted and folded in the Late Carboniferous during the Variscan Orogeny, resulting in several thin-skinned thrust units (Fig. 1A; Pérez-Estaún and Bastida 1990; Alonso and Pulgar 1995;). The main Variscan compression was followed in the Early Permian by an extensional phase (Lepvrier and Martínez-García 1990; Gutiérrez-Alonso et al. 2004), which led to fracture reactivation, crustal thinning, increased heat flow from the basement, local development of low-temperature metamorphism (Brime 1981, 1985; Aller and Brime 1985; Raven and Van der Pluijm 1986; García-López et al. 1997; Brime et al. 2001), and emplacement of small volcanic and magmatic bodies (Corretgé and Suárez 1990; Fernández-Suárez et al. 2000).

The study area, located in the southwestern Cantabrian Zone, corresponds to the central and eastern Bodón Unit (Fig. 1A), which is made up of three different thrust nappes (Marcos 1968a). From the lower to the upper these are the Forcada, the Bodón, and the Gayo nappes (Fig. 1B). The Bodón Unit is overthrusted by the Somiedo–Correcilla Unit in the south, whereas in the north it is bound by the Central Coal Basin Unit and the León Fault. The latter is an E–W oriented regional fault system, active from the Variscan onwards (Marcos 1968b; Marcos et al. 1979). The interference between the León Fault and the Bodón Unit gave rise to an important brittle shear zone, containing several non-economic dolomite-hosted mineralizations (Paniagua 1993; Paniagua et al. 1993). The first pulse of Variscan tectonism in the Bodón Unit took place in the Namurian A (Reuther 1980), whereas the main compressional event occurred in the Westphalian B and continued until the Stephanian B (Marcos 1968a).

The Bodón Unit consists of a pre-Variscan (Lower Cambrian to Lower Namurian) and a syn-Variscan (Lower Namurian to Upper Westphalian) succession (Fig. 1C); post-Variscan (Stephanian and Permian) deposits are absent. Three main carbonate formations make up the Carboniferous succession of the Bodón Unit: the Alba, Barcaliente, and Valdeteja formations. The Alba Fm. (Viséan-Namurian A) is less than 30 m thick and consists of reddish to pinkish, micritic and bioclastic nodular limestones, which pass upwards into dark gray limestones (Hemleben and Reuther 1980; Reuther 1980). The Barcaliente Fm. (Namurian A) is 200 to 350 m thick and consists of dark gray to black, well bedded and laminated, micritic and bituminous limestones (Wagner et al. 1971; Hemleben and Reuther 1980). The Valdeteja Fm. (Namurian A–B to Namurian B–Westphalian A) has a variable thickness (0 to 500 m) and is composed mainly of light grey and massive limestones, often containing bioherms (Wagner et al. 1971).

FIELD OBSERVATIONS AND SAMPLE LOCALITIES

Large volumes of Carboniferous carbonates within the Bodón Unit underwent pervasive dolomitization. The most dolomitized region corresponds to the middle of the study area (Villanueva de la Tercia, Mina Profunda, Cármenes; Fig 1B), where precursor limestones are only rarely preserved. Towards the eastern and western extremities of the study area the amount of dolomite decreases and remnants of limestones become progressively more common. The sediments most affected by dolomitization belong to the Barcaliente and Valdeteja fms., though extensive dolomite occurrences are found also in the uppermost member of the underlying Alba Fm.

The dolomites appear as extremely irregular, yellowish-brown to dark gray masses, which enclose remnants of light gray precursor limestones (Fig. 2A). Dolomite bodies may be spatially related to rock discontinuities such as faults, fractures, and bedding planes. The dolomite–limestone contacts are very sharp and generally cut primary features such as bedding planes and sedimentary structures (Fig. 2B). All of these features are commonly accepted as criteria for late diagenetic dolomitization (compare with Morrow et al. 1990, Coniglio et al. 1994, and Machel 2005).

Different dolomite types can be recognized in hand specimens. Samples from the lower Barcaliente Fm. may exhibit a banding, given by the

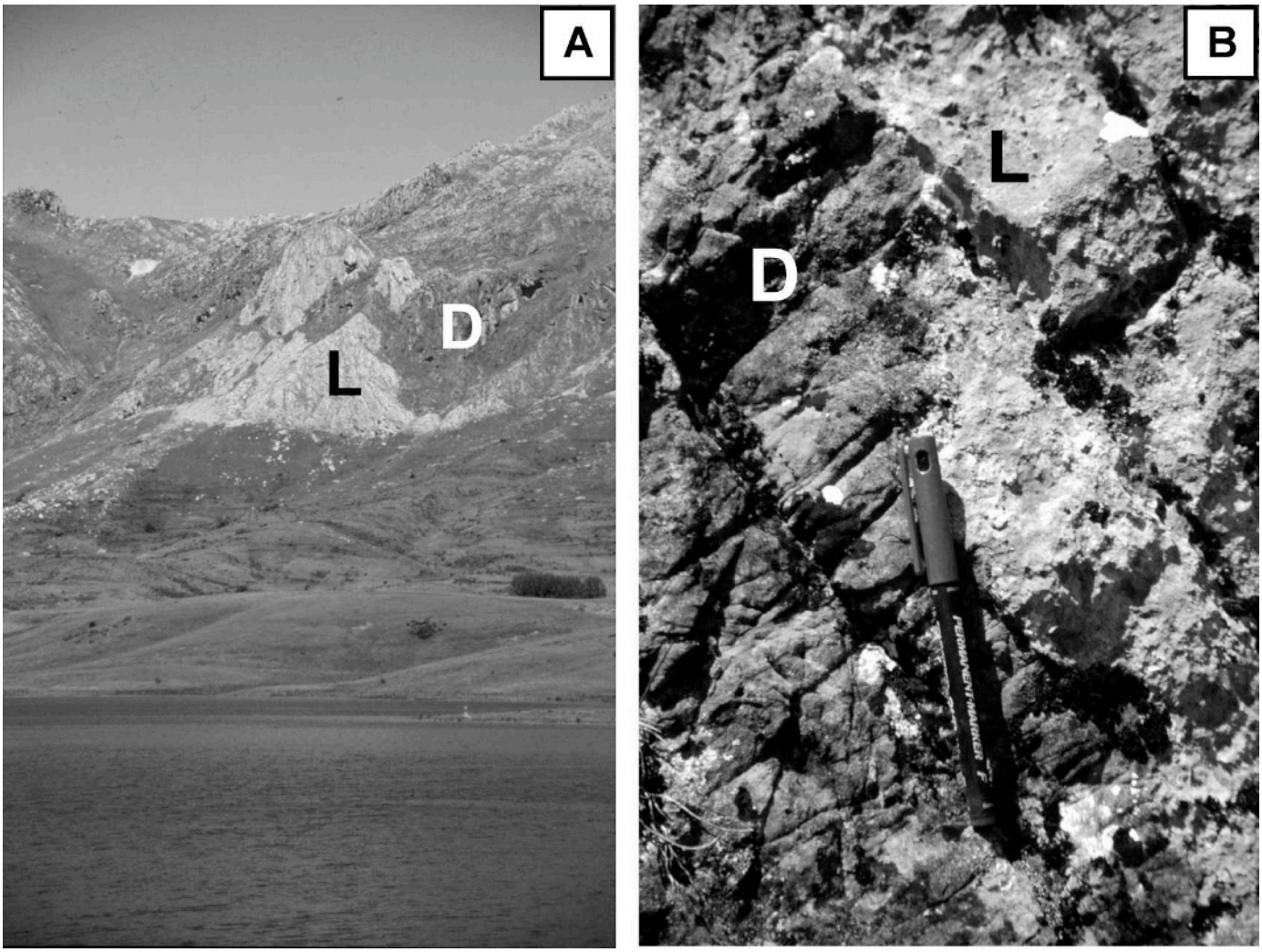

FIG. 2.—**A)** Dolomites (D) occur in the field as irregular masses, which enclose remnants of precursor limestones (L) as relic bodies (20–50 m wide). Note the color contrast between the dark gray dolomites and the light gray limestones. **B)** Sharp contact between precursor limestone (L) and dolomite (D) cuts the trace of bedding planes. The more brittle rheology of the dolomite is witnessed by fractures, which do not propagate into the limestone. Scale (marker pen) is 14 cm.

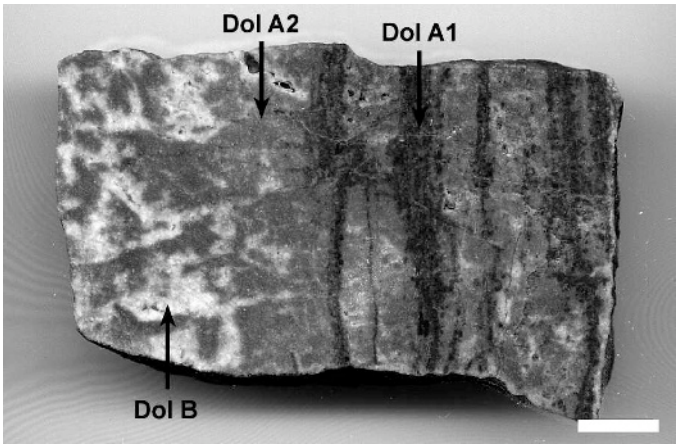

FIG. 3.—Rock sample (CuBD1M, Barcaliente Fm., Cubillas de Arbas) showing the coexistence of three different dolomite types. *Dol A1* (dark gray) and *Dol A2* (light gray) occur as stratiform bands, whereas *Dol B* (white) fills small cavities hosted in *Dol A2*. Scale bar is 1 cm.

alternation of differently colored dolomite bands, roughly parallel to the bedding planes (Fig. 3). Typically, the darker bands (*Dol A1*) are arranged on both sides of lamination- or bedding-parallel stylolite planes, whereas the lighter bands (*Dol A2*) are found within specific bands of stratification. Both *Dol A1* and *Dol A2* consist of a mosaic of dolomite crystals and are replacive in origin inasmuch as they locally preserve primary textures of the precursor limestones (e.g., fossil fragments). *Dol A2*, frequently the only mosaic dolomite to be observed, hosts widespread and variously oriented cavities, partly filled with sparry dolomite (*Dol B*; Fig. 3). *Dol B* is milky white and mostly of the saddle type, as indicated by curved crystal faces. It is a void-filling phase inasmuch as it occurs as pore or fracture filling and it does not preserve primary features of the precursors. *Dol A2* and *Dol B* may form peculiar structures, frequently reported as "zebra-structures" or "zebra dolomites" (e.g., Wallace et al. 1994; Nielsen et al. 1998). These are represented by the rhythmic repetition (Fig. 4A) of millimeter-scale *Dol A2* and *Dol B* sheets, with open space between two subsequent *Dol B* sheets. In other cases the remaining voids are filled by coarsely crystalline calcites, the milky white *Cal 1* (Fig. 4B) and the transparent *Cal 2*.

Dolomitization postdated the main compressional phase of the Variscan deformation in the study area (Westphalian B–Stephanian B;

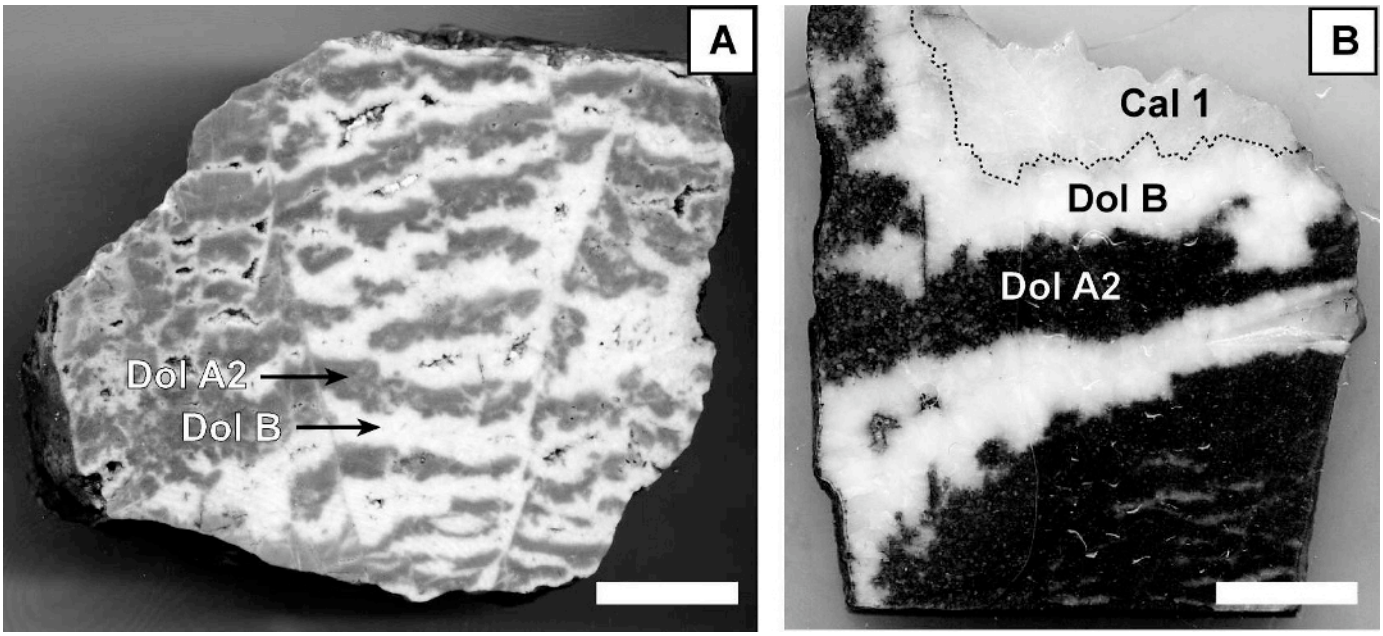

FIG. 4.—**A)** Rock sample (CaBD2B, Barcaliente Fm., Carmenes) showing *Dol A2* and *Dol B* sheets forming "zebra structures." Small voids are left open between two subsequent *Dol B* sheets. Scale bar is 2 cm. **B)** Rock slab showing zebra structures. Milky white *Cal 1* fills the cavities lined by *Dol B*. Scale bar is 1 cm.

Marcos 1968a) and predated the mineralizing event (Early Permian; Paniagua 1993; Paniagua et al. 1993). This is deduced mainly from the occurrence of undeformed dolomites close to tectonic lineaments of Variscan age, the absence of dolomitization in carbonate clasts derived from the erosion of Barcaliente and Valdeteja Fms. within continental Stephanian B conglomerates, and the presence of Early Permian ore mineral assemblages in the dolomite porosity (for details see Gasparrini 2003, Gasparrini et al. in press).

Macroscopic and microscopic observations of the dolomite–calcite phase assemblages were made on rock samples collected at various localities in the area illustrated in Figure 1B and from various formations of the Carboniferous succession. Eight of these samples, suitable for fluid-inclusion investigation, were selected to prepare thick sections; location, formation of provenance, and phase assemblage of these samples are summarized in Table 1.

ANALYTICAL METHODS

Microthermometry

The fluid inclusion study was conducted on double polished 100–120 µm thick sections prepared with a cold technique, such that the maximal temperature reached was about 35°C, in order to prevent reequilibration and/or decrepitation of the inclusions. Microthermometry measurements were carried out using either a Linkam TH 600 or a Linkam MDS 600 heating–freezing stage. Calibration was performed using synthetic fluid inclusions at −56.6 (CO_2), 0.0 and 374.0°C (H_2O), and chemical standards at 99.2 ($C_{14}H_{10}$) and 212.0°C ($AgNO_3$). The accuracy of the data is approximately ± 0.4 degree below −60°C, ± 0.2 between −60 and + 100°C, and ± 1.0 above 100°C. Homogenization measurements were carried out before freezing runs to avoid stretching of fluid inclusions by ice nucleation.

The volumetric proportion of the liquid phase at room temperature relative to the total volume of the fluid inclusions, referred as φ_{liq}, was calculated from screen images by measuring areas, according to the considerations of Bakker and Diamond (2006). This study illustrates that above φ_{liq} = 0.9 the area fraction is nearly equal to volume fraction, ± 4% of the measured fraction.

Raman Spectroscopy

Liquid and gas phases in the fluid inclusions were analyzed by a LABRAM confocal-Raman spectrometer using a 100 mW frequency-doubled Nd-YAG laser. A 532.2 nm wavelength (green laser) was used for radiation on both dolomite and calcite samples. In many samples the fluid inclusions were too small and flat to accomplish Raman spectroscopy. The measurements were performed at room temperature

TABLE 1.—*Location of the sampled sites (from the western- to the easternmost) in the Bodón Unit with sample names, host formations and mineral assemblage encountered.*

Locality	Position	Formation	Sample	Mineral assemblage
1. Caldas de Luna	N 42°56′150″, W 5°50′606″, 1225 m	Alba (top)	136	Dol A2, Dol B, Cal 1
2. Cubillas de Arbas	N 42°56′725″, W 5°48′165″, 1785 m	Barcaliente (middle)	CuBD1M	Dol A1, Dol A2, Dol B
3. Villanueva de la Tercia	N 42°58′674″, W 5°40′982″, 1215 m	Alba (top)	VC-172	Dol A2, Dol B, Cal 1
4. Villanueva de la Tercia	N 42°58′674″, W 5°40′982″, 1215 m	Barcaliente (base)	VCBD1B	Dol A2, Dol B, Cal 1
5. Mina Profonda	N 42°57′981″, W 5°36′576″, 1650 m	Barcaliente (middle)	MPBD2M	Dol A2, Dol B, Cal 1
6. Cármenes	N 42°58′331″, W 5°34′452″, 1450 m	Barcaliente (base)	CaBD2B	Dol A2, Dol B, Cal 2
7. Canseco	N 42°58′825″, W 5°32′444″, 1260 m	Barcaliente (top)	45	Dol A2, Dol B, Cal 1
8. Nocedo de Curueño	N 42°53′905″, W 5°23′835″, 1075 m	Valdeteja (base)	NVD1B	Dol A2, Dol B, Cal 2

on fluid inclusions near to the sample surface. Raman spectra from the liquid phases revealed a broad band between 3000 and 3700 cm^{-1}, with a principal peak at about 3400 cm^{-1}, typical of aqueous solutions (e.g., Mernagh and Wilde 1989; Bakker 2004). Raman measurements on the vapor phase could not detect gases, such as CO_2, CO, CH_4, N_2, and H_2, suggesting that the bubbles consist mainly of water vapor. The investigated fluid inclusions do not emit fluorescence under either UV light or laser light, indicating the absence of oil.

Combined Raman Spectroscopy and Microthermometry

A Linkam TMS 93 stage attached to a Raman microprobe enabled spectroscopic analysis at selected temperatures. Raman spectra were recorded at temperatures below −170°C in order to identify ice and salt hydrates (ice-like phases), which were obtained by freezing the fluid inclusions (see Dubessy et al. 1982; Bakker 2004). The Raman signal of the phases within the inclusions was obtained by subtracting the background signal of the host mineral, measured at each selected temperature (see Bakker 2004). Subsequently, these spectra were analyzed for the peak positions and compared with already compiled tables for the most common substances (Samson and Walker 2000; Bakker 2002; Bakker 2004). Exact melting temperatures of individual ice-like phases were obtained by Raman measurements during heating runs with the Linkam stage.

Large metastabilities of phase assemblages may exist in saline aqueous solutions within fluid inclusions (Bakker 2004). Many of the studied inclusions did not nucleate ice-like phases after rapid cooling down to −196°C at all. Subsequently fast heating towards −60°C did not result in salt-hydrate nucleation: though the inclusions appeared completely frozen, ice and a highly saline aqueous liquid were metastably present. In contrast, slow and stepwise cycling towards −60°C, with intervals of constant low temperatures, resulted in the formation of complex salt hydrates and ice. Demixing of these salt hydrates and growth of individual salt-hydrate crystals was obtained by further temperature cycling.

Salinity Expression

Calculation of salinities is based on the equivalent mass % principle. Generally these calculations use NaCl (e.g., Roedder 1984), but this study uses $CaCl_2$ (Bakker 2003), in order to express ice and salt hydrate melting temperatures below the H_2O–NaCl eutectic point (−21.1°C). Equivalent mass % is a purely arbitrary way of reproducing the melting temperature of ice, salts, and salt hydrates, and it does not contain any information about the real composition of the aqueous solution. Therefore, it is an expression of temperature.

Thermodynamic models of complex highly saline H_2O–salt systems are not available (Bakker 2003). Only some purely empirical equations exist for the H_2O–KCl–NaCl system, and only partly for the H_2O–NaCl–$CaCl_2$ and the H_2O–NaCl–$MgCl_2$ systems. Because of the lack of models, salinity calculations are based on the equivalent mass % principle within the H_2O–NaCl–$CaCl_2$ ternary system, using the melting temperatures of both ice and hydrohalite.

Thermodynamic Calculations and Computer Programs

The microthermometry and Raman data were used to determine bulk composition and density of the fluids trapped within the inclusions, by means of the computer package *FLUIDS* (Bakker 2003). Salinities were calculated in the binary H_2O–$CaCl_2$ and ternary H_2O–NaCl–$CaCl_2$ systems (Naden 1996), using the program *AqSo2* from the package *FLUIDS*. The program *BULK* enabled the calculation of bulk fluid properties (i.e., bulk composition and density) of individual fluid inclusions. The calculation was accomplished using a purely empirical thermodynamic model, the equation of state for electrolyte-bearing aqueous solutions of Krumgalz et al. (1996) and the volume fractions of the liquid phase of the inclusions at room temperature. The isochore slopes were calculated by means of the program *Loner 38* (Zhang and Frantz 1987), whose requirement is the knowledge of homogenization temperature (T_h) and salinity of the inclusions.

PETROGRAPHY OF THE DOLOMITE AND CALCITE PHASES

The spatial relationships between the observed dolomite and calcite phases in hand specimens is illustrated in Figures 3 and 4. According to the dolomite texture classification of Sibley and Gregg (1987) the replacive *Dol A1* and *Dol A2* can be defined as nonplanar, inasmuch as they consist of anhedral and closely packed crystals with lobate or curved intercrystalline boundaries (Fig. 5A). The crystals are irregularly coated by a brownish amorphous material, which represents the residue of leaching of the precursor limestones during dolomitization. These dolomites are strongly fabric destructive as they obliterated depositional and diagenetic features of the precursor limestones and fossils are preserved only as recrystallized relics.

Dol A1 crystals have a pale brown color and undulose extinction. A common crystal size distribution consists of fine crystals (10–20 μm), which become coarser (up to 80 μm) towards discontinuities (i.e., lamination and stylolite planes). *Dol A2* crystals (50–200 μm) are volumetrically dominant and have a lighter color. Coarser *Dol A2* crystals have an undulose extinction under crossed-polarized light, typical of saddle dolomite (Radke and Mathis 1980; Spötl and Pitman 1998), whereas finer crystals have only undulose extinction. The transition from *Dol A1* towards *Dol A2* is gradual: *Dol A1* crystals become less abundant with increasing distance from the discontinuity planes until they appear scattered within the mosaic of *Dol A2* crystals.

The void-filling *Dol B* lines cavities hosted in *Dol A2. Dol B* crystals are interlocked, coarse to very coarse crystalline (0.2–2 mm), nonplanar to planar-s (*sensu* Sibley and Gregg 1987), and always display undulose extinction of saddle dolomite (Fig. 5A). They are more transparent than the replacive dolomite crystals, inasmuch as they lack coatings of impurities. The contact between *Dol B* and the replacive dolomites does not correspond to a reaction boundary, because abrasive, moat, and corona textures are not observed. *Dol B* crystals become coarser from the first crystal generation, following the replacive *Dol A2*, to the last crystal generation, close to the cavities (Fig. 5A). The final growth stage of *Dol B* consists of millimeter-size dolomite crystals (Fig. 5), whose shape ranges from rhombohedral with straight boundaries to symmetrical saddle forms.

Cal 1 and *Cal 2* postdated the dolomites, because they fill cavities lined by *Dol B* crystals. They are very coarse (1–5 mm), blocky and xenotopic calcites, characterized by sharp extinction and compromise boundaries between adjacent crystals. *Cal 1* is commonly twinned, whereas *Cal 2* is not. Reaction boundaries are not observed between *Cal 1* and *Dol B* (Fig. 5B). In contrast, *Dol B* crystals appear corroded at the contact with *Cal 2*.

The textural relationships point to a succession of diagenetic events comprising a first replacement of the precursor limestones by *Dol A1* and *Dol A2*, followed by precipitation of the void-filling *Dol B*, and later precipitation of two distinct calcite cements.

FLUID-INCLUSION STUDY

Fluid-Inclusion Petrography

A detailed petrographic study of the dolomite and calcite phases reveal the presence of several types of fluid inclusions. The location and distribution of the inclusions within the various mineral phases is illustrated schematically in Figure 6. The petrographic features of the main inclusion types are summarized in Table 2.

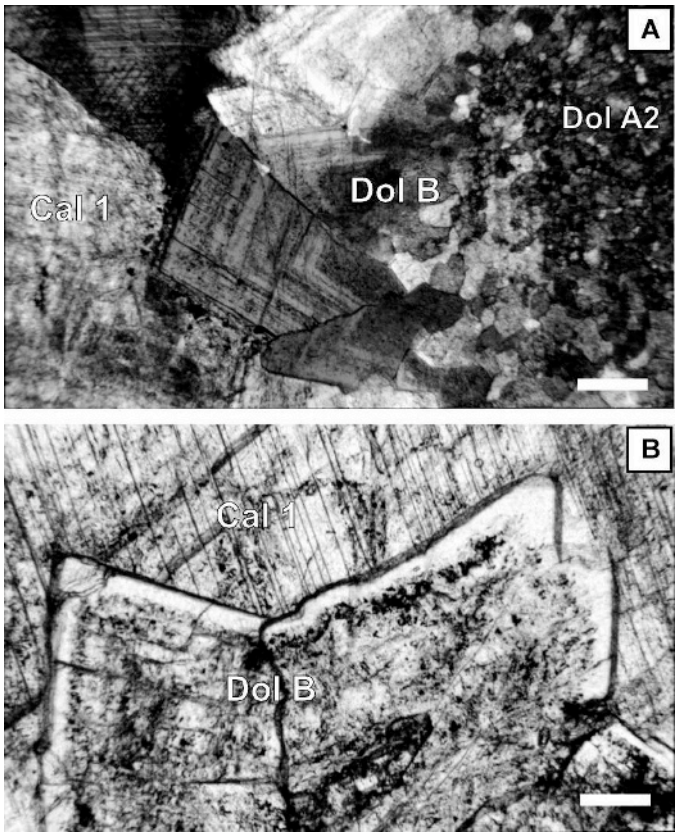

FIG. 5.— Photomicrographs showing the spatial and textural relationships of the dolomite–calcite phase assemblage. **A)** The dolomite crystal size increases from the replacive (*Dol A2*) towards the void-filling (*Dol B*) phases. No reaction boundaries exist between the different dolomites. *Dol B* crystals display sweeping extinction and are in contact with twinned crystals of *Cal 1*. Scale bar is 0.4 mm. Cross-polarized light. Rock sample: 136, Alba Fm., Caldes de Luna. **B)** Last crystal generation of *Dol B* in contact with twinned *Cal 1* crystals. Dol B crystals have straight boundaries and exhibit cloudy, inclusion-rich cores and clear, inclusion-free most external rims. Scale bar is 0.2 mm. Plane light. Rock sample: 45, Barcaliente Fm., Canseco.

Dol A1 crystals display a uniform cloudiness due to the presence of small (< 1 μm), probable primary fluid inclusions densely distributed throughout individual crystals (Fig. 6A). Owing to the small size and the dark color of the crystals, inclusions suitable for microthermometric measurements were not found.

Fluid inclusions in *Dol A2* crystals are densely distributed in three dimensions and are concentrated mainly in the crystal cores (Fig. 6B), pointing to a primary origin. These inclusions (type I) are up to 5 μm in length and have an irregular shape, which may mimic the crystallographic directions of the host crystal, or alternatively they may have a negative crystal shape. Type I inclusions are two-phase and liquid-rich with φ_{liq} between 0.83 and 0.96 (mode at 0.95).

Dol B crystals commonly host uniformly distributed fluid inclusions (type II). Locally, the crystals have inclusion-rich cores and clear inclusion-free rims. Type II inclusions have an irregular to lobate shape and are two-phase and liquid-rich. φ_{liq} ranges form 0.78 to 0.97 (mode at 0.95). The larger type II inclusions (up to 18 μm in length) occur in the final crystal generation of *Dol B* and are preferentially grouped in the crystal cores or along crystal growth zones (Figs. 6C, 7A, B)

Cal 1 is characterized by abundant primary fluid inclusions (type III) mostly confined by concentric growth-zone boundaries, though they also occur isolated or grouped in clusters (Figs. 6D, 7C, D). Type III inclusions are up to 20 μm in length, spheroidal to oblate in shape, two-phase, and liquid-rich. φ_{liq} varies between 0.83 and 0.97 (mode at 0.95). Secondary fluid inclusions (type I*V*) are less frequently observed in *Cal 1*. They are located along trails and seal fractures, especially in heavily twinned crystals. They are less than 2 μm in length, spheroidal in shape, single-phase (all liquid), and were never observed in the dolomite crystals. Therefore, type IV inclusions were not considered in the present study.

Fluid inclusions in *Cal 2* (type V) are isolated and do not occur either along growth zones or along trails. Type V inclusions are single-phase (all liquid) but they frequently appear empty (Figs. 6E, 7E), due to the leakage of the liquid phase during section preparation procedures. They are up to 30 μm in length and have an irregular shape, with crystallographically controlled inclusion walls (Fig. 7E). Negative crystal shapes are also common. These inclusions are considered to be of primary origin. Raman spectroscopy reveals the presence of a nearly pure H_2O fluid. Microthermometry was not applied to these inclusions.

Standard Microthermometry Results

The fluids in types I, II, and III inclusions can be characterized in an H_2O-salt system. The main results of microthermometry are summarized in Table 2. A complete database of microthermometry data can be found in the Appendix 1 (see Acknowledgments section). Types I, II, and III inclusions have a narrow range of filling degrees (φ_{liq}), suggesting homogeneous trapping. Total homogenization occurred in the liquid phase for all inclusion types. Occasionally after total homogenization in *types I* and *II* inclusions in *Dol A2* and *Dol B*, the vapor bubble was metastably absent at room temperature. Ice nucleation was not observed during the first cooling run down to −196°C, indicating a significant amount of metastability. These inclusions nucleated vapor and ice-like phases only after reheating towards −60°C. The freezing behavior of the majority of type III inclusions in *Cal 1* is significantly different, as ice-like phases nucleated during the first cooling run, at temperatures below −60°C. The presence of a first liquid phase during reheating was deduced optically from an abrupt movement or a gradual expansion of the vapor bubble. The corresponding temperatures, reported in Table 2 as T_{liq}, represent the upper constraints to the true eutectic temperatures (T_e). In most fluid inclusions only the final melting temperatures (T_m) could be determined, presumably corresponding to the melting of ice.

In *Dol A2*, 92% of all T_h data for type I inclusions falls in the range 100–140°C. The frequency histogram shows an asymmetric distribution of the T_h data, with mode between 130 and 140°C (Table 2, Fig. 8). In the Bodón Nappe no significant differences in T_h exist between the central part (Villanueva de la Tercia) and the western part (Caldas de Luna) (Fig. 8A). Slightly lower T_h values were recorded in the sample from the Forcada Nappe (Canseco). The distribution of all T_m data has a pronounced mode at −34°C (Table 2, Fig. 9). The limited variation in T_m together with the relatively high salinity of *type I* inclusions is recorded from the whole Bodón Unit. The salinity of type I inclusions varies in the narrow range 25.5–27.0 eq. mass % $CaCl_2$ (mode at 27 eq. mass%). The T_h–T_m plot (Fig. 10A) underlines the similar salinity in all type I inclusions for a relatively larger spread of the T_h values.

In Dol B, 95% of the T_h data for type II inclusions falls in the range 100–150°C (Table 2, Fig. 8B). The histogram shows normal Gaussian distributions of the T_h data for each locality. Type II inclusions record a variation in T_h from one locality to another (Fig. 11). Higher T_h values were measured in samples coming from localities in the centre of the Bodón Nappe, i.e., Cármenes (range 146.0–205.5°C and mode at 150°C), Villanueva de la Tercia (range 113.0–155.0°C and mode at 140°C) and Mina Profunda (range 93.1–158.8°C and mode at 130°C). Lower T_h values were measured in samples collected from western localities of the Bodón Nappe, i.e., Caldas de Luna (range 99.2–143.7°C and mode at 110°C) and Cubillas de Arbas (range 95.8–114.9°C and mode at 110°C).

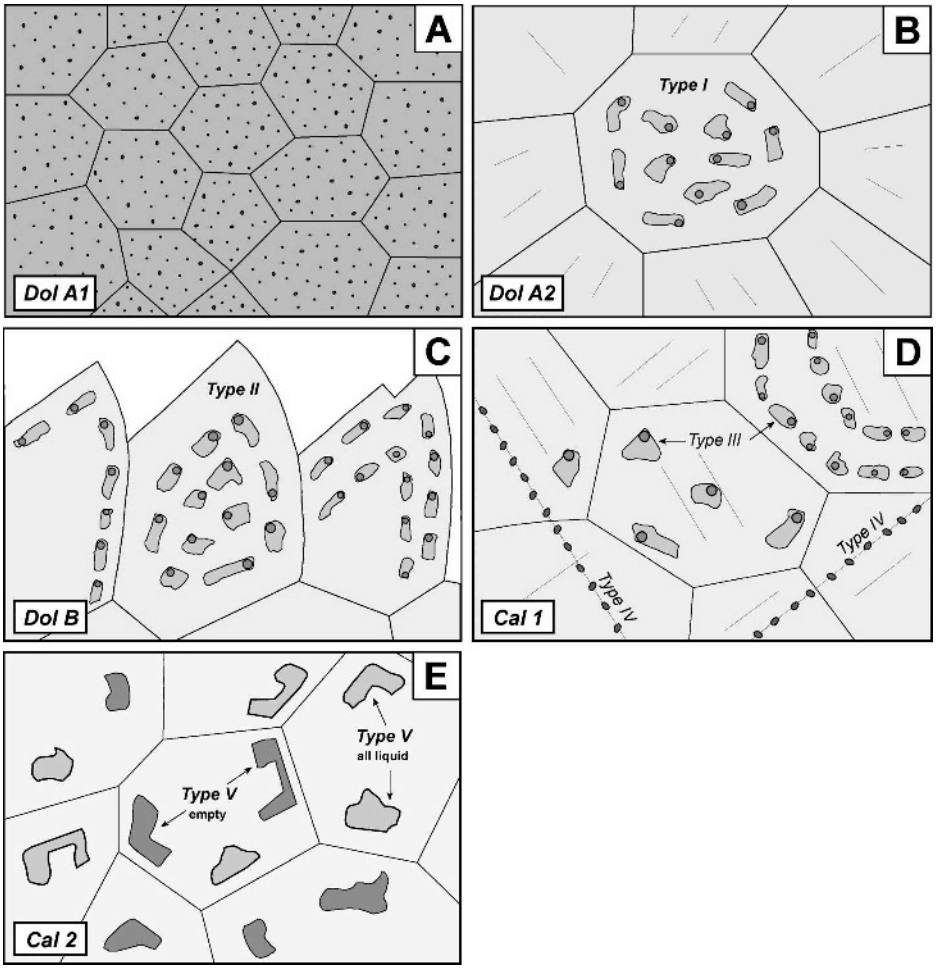

FIG. 6.—Sketch illustrating the location and distribution of the fluid inclusions in the various mineral phases. **A)** Tiny inclusions in *Dol A1*. **B)** Type I inclusions in *Dol A2*. **C)** Type II inclusions in the last crystal generation of *Dol B*. **D)** Type III and IV inclusions in *Cal 1*. **E)** Type V inclusions in *Cal 2*.

Similarly, slightly lower T_h values were also recorded in samples collected from eastern localities, in the Gayo and Forcada nappes, e.g., Nocedo de Curueño (range 118.5–139.8°C and mode at 125°C). The variation in T_m between different localities for type II inclusions is slightly higher than for type I inclusions (Fig. 9B, Table 2). In the western part of the Bodón Nappe, modes of −36°C and −30°C are obtained for Cubillas de Arbas and Caldas de Luna, respectively, whereas in the center of the Bodón Nappe a mode of −34°C is recorded at Villanueva de la Tercia. Type II inclusions have salinities between 23.7 and 29.2 eq. mass % $CaCl_2$. The value of the salinity mode is similar to that of type I inclusions: 27 eq. mass % $CaCl_2$. The salinity variation between localities might reflect a minor local variation in fluid chemistry. The T_h–T_m plot (Fig. 10B) defines different groups of fluids, corresponding to different localities in the western part of the studied area, whereas the eastern and central parts display a narrow variation in fluid properties.

In *Cal 1*, 94 % of the T_h data for type III inclusions falls in the range 100–130°C, with a well-defined mode at 115°C (Fig. 8C, Table 2). The T_m data have an asymmetric distribution in the range of −18 to −26°C, with a mode value at −24°C (Fig. 9C, Table 2). The salinity of type III inclusions is slightly lower than that of type I and II and ranges between 20.3 and 23.4 eq. mass % $CaCl_2$. The mode value is 23 eq. mass % $CaCl_2$. Both T_h and T_m values for type III inclusions are significant distinct from those measured in the dolomites (Fig. 10). Type III inclusions do not show a compositional variation between various localities, judging by microthermometrical behavior.

The calculated bulk density of types I, II, and III inclusions are reported in Appendix 1 (see Acknowledgments section). The molar volume (V_m) of *type I* inclusions ranges between 17.81 and 20.25 cm^3/mol. Type II and III inclusions have similar V_m between 17.28 and 20.66 cm^3/mol, and between 17.33 and 19.58 cm^3/mol, respectively.

Comparison with Cryo-Raman Spectroscopy

Low-temperature microthermometry experiments in combination with Raman spectroscopy enabled the determination of individual phase and phase changes, i.e., the melting of individual ice and salt hydrates, which could not be obtained by optical means alone.

Four individual type II fluid inclusions in *Dol B* (sample VCBD1B; Table 1) were selected to illustrate different melting behaviors due to different cooling–heating procedures (Table 3). The fast-cycling procedure did not nucleate salt hydrates but produced a metastable mixture of ice and a highly saline brine. These inclusions had a melting behavior similar to that of the inclusions investigated by microthermometry only (cf. Table 2 and Table 3). Ice melting in the range of −28.0 to −35.0°C corresponds to a salinity of 24.0–26.5 eq. mass% $CaCl_2$. In terms of chloridity the same salinity can be expressed as 16.8–18.7 eq. mass% Cl^-. Slow and stepwise cycling resulted in the nucleation of ice and several salt hydrates. The inclusions displayed a complex melting history of these phases, and they revealed higher T_m(ice) values in the presence of presumably stable phase assemblages (see Table 3). The eutectic

TABLE 2.—*Petrographic features of the main types of fluid inclusions. The inclusion size is given as length in μm. φ_{liq} stands for the volume fraction of the liquid phase at room temperature relative to the total volume of the fluid inclusion. The table also summarises the results of microthermometry for* type I, II *and* III *inclusions. The range and mode values of T_h, T_{liq} and T_m are reported. In brackets is the number of measurements accomplished for each of the three parameters.*

Mineral phase	Inclusion type	Phases	Shape	Size (μm)	ϕ_{liq}	T_h (°C)		T_{liq} (°C)		T_m (°C)	
						mode	range	mode	range	mode	range
Dol A2	*I*	aqueous liquid, vapor bubble	irregular to negative crystal	< 5	0.83/0.96	130–140 (26)	78.8/196.5	−48 (7)	−31.0/51.5	−34 (19)	−32.0/−36.5
Dol B	*II*	aqueous liquid, vapor bubble	irregular to lobate	up to 18	0.78/0.97	130 (147)	93.1/205.5	−40 (58)	−32.5/−52.8	−34 (119)	−27.1/−39.5
Cal 1	*III*	aqueous liquid, vapor bubble	spheroidal to lobate	up to 20	0.83/0.97	115 (32)	100.0/145.6	−34 (15)	−28.5/−46.9	−24 (28)	−19.5/−26.5
	IV	aqueous liquid	spheroidal (along trails)	< 2	1	—	—	—	—	—	—
Cal 2	*V*	aqueous liquid (or empty)	irregular to negative crystal	up to 30	1	—	—	—	—	—	—

temperature (T_e) of the fluid system is between −50 and −57°C, as shown by the reappearance of the Raman spectrum of water. Simultaneously, an unknown salt hydrate must have disappeared at this temperature, although it was not detected by Raman spectroscopy. A second salt hydrate with a well defined Raman spectrum melted at temperatures between −41.3 and −43.3°C. On further heating, ice and hydrohalite crystals could be distinguished optically in only some inclusions. Ice melted at temperatures between −22.0 and −33.2°C. Hydrohalite melted last at temperatures between −10.5 and −18.1°C (Table 3). The calculated salinity in these type II inclusions is highly variable, inasmuch as $CaCl_2$ ranges between 0.4 and 21.9 eq. mass %, and NaCl ranges between 6.7 and 25.0 eq. mass %, and differs significantly from those previously calculated in the same inclusions. The chloridity of this solution can be expressed as 17.0–18.2 eq. mass% Cl^-, and is similar to the results from the fast cooling cycle. However, the equivalent mole fraction of NaCl in the salt mixture is highly variable, ranging from 0.233 to 0.983 (Table 3). In conclusion, depending on the cooling procedure, type II inclusions in *Dol B* had different melting behaviors. After fast cycling, ice in the presence of only a brine melted at significantly lower temperatures than when ice coexisted with salt hydrates. This is a consequence of the greater freezing-point depression of ice within more saline solutions. In smaller fluid inclusions (< 10 μm) ice can be easily mistaken for hydrohalite, which may lead to erroneous salinity calculations (see also Bakker 2004).

*Raman Spectra of Salt Hydrates in Type II Inclusions (*Dol B*)*

The Raman spectra within type II fluid inclusions in *Dol B* (Fig. 12) obtained after a first stepwise cooling procedure cannot be attributed to any of the most common simple salt hydrates (cf. Dubessy et al. 1982; Samson and Walker 2000; Bakker 2004). They possibly correspond to an unknown complex salt hydrate, which is a solid solution between the various cations (e.g., Na–K–Ca–Mg) dissolved in the aqueous fluid and bonded to chlorine in hydrated crystals. Spectra of this kind are systematically obtained from all type II inclusions after the same cooling procedure. A variety of intensities for each individual peak at a selected temperature was observed (Fig. 12), which is a consequence of different crystallographic orientations of salt-hydrate crystals relative to the polarization of the Raman laser.

Demixing of this complex and possibly metastable salt-hydrate solid solution and growing of large crystals of individual salt-hydrate components were obtained by subsequent temperature cycling experiments (Figs. 13, 14, Table 4). They display peak positions (Δv) different from the first-formed complex salt hydrate (Fig. 12). Single crystals of hydrohalite were isolated and measured in different orientations (Fig. 13, Table 4), resulting in a variable relative intensity of individual peaks. Additional spectra were recorded from other salt-hydrate crystals (Fig. 14, and X in Table 4). Although the pattern of the obtained group of peaks is similar to $MgCl_2 \cdot 12H_2O$, the peak positions are systematically shifted by 5 cm^{-1} to lower values. Peak positions may be shifted by several wave numbers because of the presence of other types of salt hydrates within the inclusions (see also Bakker 2004). A third type of salt hydrate was detected but could not be further characterized (lower spectrum in Fig. 14 and Y in Table 4). Further studies are needed to identify the components in these salt hydrates. Salt hydrates of $CaCl_2$ or other components with a low mole fraction in the aqueous solution were not detected after recrystallization of the complex salt hydrate. They either are present in minor amounts in a residual aqueous liquid solution or were nondetectably incorporated in the salt hydrates of the major components.

Raman Spectra of Salt Hydrates in Type III Inclusions (Cal 1)

Type III inclusions in *Cal 1* from Mina Profunda (sample MPBD2M, Table 1) nucleated ice-like phases during the first cooling run and developed coarse crystallinity when kept for a few minutes at temperatures as low as −60°C. Raman spectra at −170°C indicated the presence of only ice and hydrohalite. Raman measurements during reheating indicated the presence of a first liquid at temperatures between −46 and −50°C. These low values suggest the presence of other salt types in addition of NaCl, which could not be further characterized. Only minor amounts of unknown salts, possibly $CaCl_2$ and $MgCl_2$, would be responsible for the observed low T_e values. Only in larger inclusions (> 10 μm) could ice and hydrohalite be distinguished optically during reheating (Fig. 15). The sequence of phase changes in one of these type III inclusions during a heating–freezing cycle is shown in Figure 15. Ice crystals typically melted first, at temperatures between −21.5 and −24.7°C, with hydrohalite being the last phase to melt at temperatures between −16.3 and −24.0°C. The calculated salinity of type III inclusions in *Cal 1* is 7.4 to 10.0 eq. mass% $CaCl_2$ and 16.1 to 17.8 eq. mass % NaCl. This fluid is less saline than the fluid trapped within the dolomite crystals. The nearly constant mole ratio of NaCl and $CaCl_2$ (3.7 to 4.6) in calcite inclusions possibly reflects a homogeneous source for the salts.

Using microthermometry alone no distinction between ice and hydrohalite crystals could be made in smaller fluid inclusions (< 10 μm). Assuming ice to be the last phase to melt may result, therefore, in an underestimation of the salinity of type III inclusions.

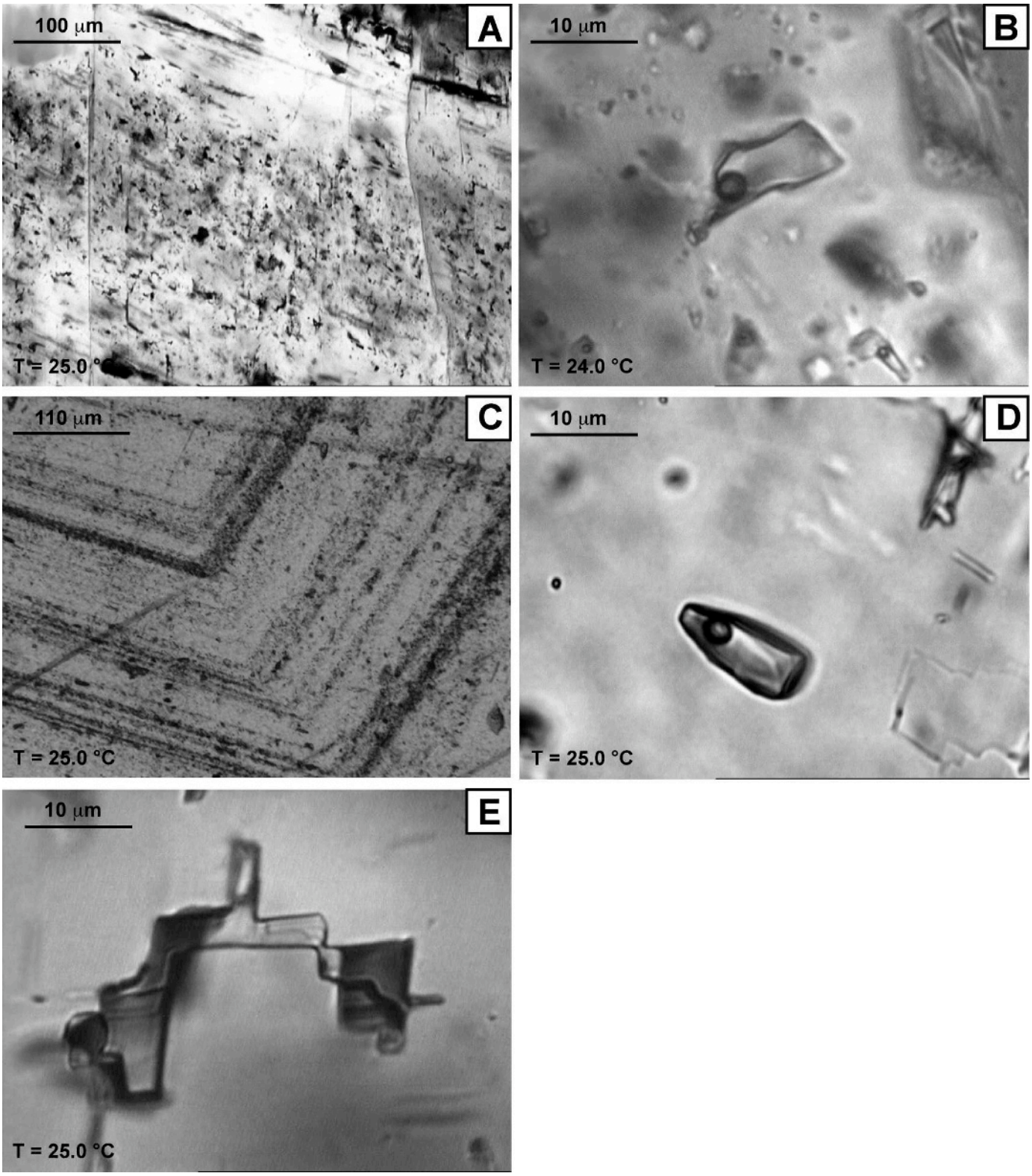

FIG. 7.—Photomicrographs of fluid inclusions in the various mineral phases. **A)** Type II inclusions in *Dol B* along a growth zone. **B)** Detail of a type II inclusion. **C)** Type III inclusions in *Cal 1* along growth-zone boundaries. **D)** Detail of a type III inclusion. **E)** Isolated Type V inclusion in *Cal 2* with crystallographically controlled walls.

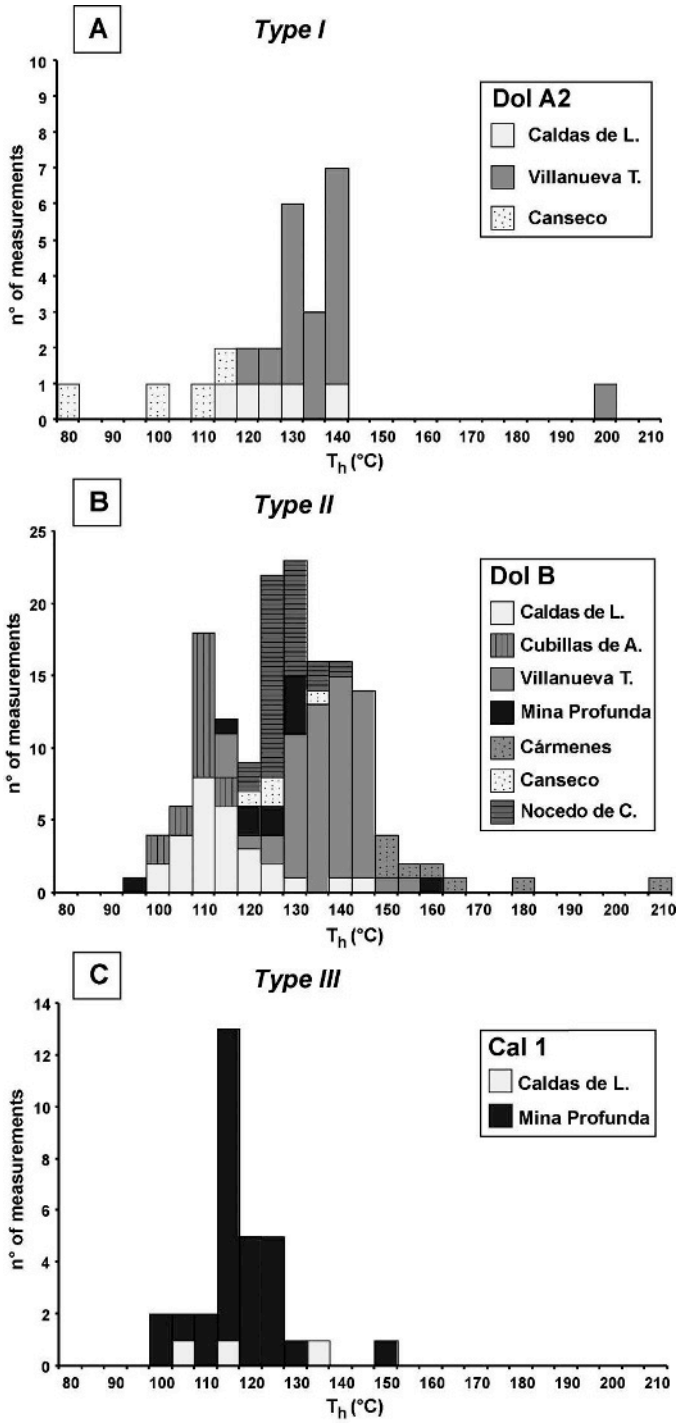

FIG. 8.—Histograms showing the frequency distribution of T_h values. **A)** Type I inclusions in *Dol A2*. **B)** Type III inclusions in *Dol B*. **C)** Type IV inclusions in *Cal 1*.

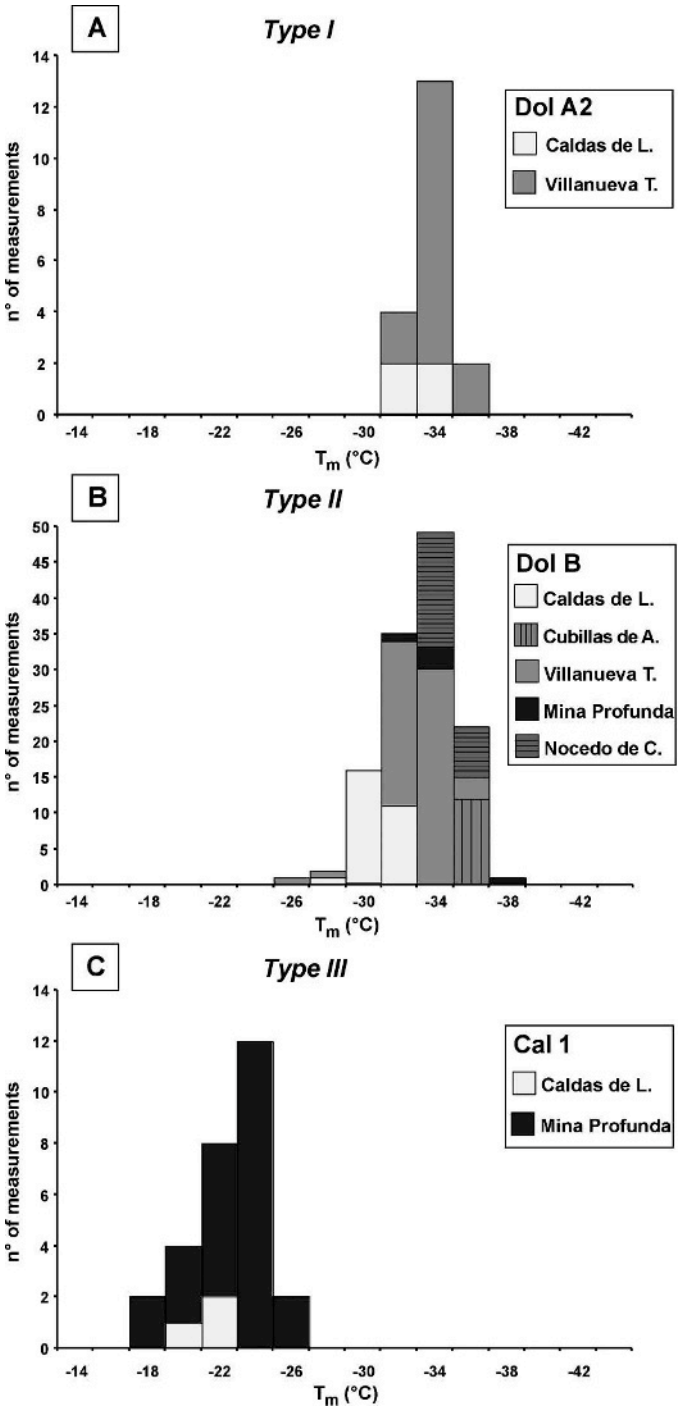

FIG. 9.—Histograms showing the frequency distribution of T_m values. **A)** Type I inclusions in *Dol A2*. **B)** Type II inclusions in *Dol B*. **C)** Type III inclusions in *Cal 1*.

DISCUSSION

Salinity of the Entrapped Fluids

Microthermometry and Raman spectroscopy indicate that the fluids in both dolomite and calcite crystals can be characterized in an H_2O–salt system. Despite morphological differences, microthermometry results illustrate the similarities between the primary fluid inclusions in *Dol A2* and *Dol B*. This means that type I and type II inclusions have possibly formed from fluid of the same composition (i.e., salinity) and similar temperature and density. The complexity of the salt system is illustrated by combined Raman spectroscopy and microthermometry: at least three different types of salt species could be detected from their salt hydrates, of which only NaCl could be positively identified. The salinity calculations are based on the equivalent mass% principle. The obtained variation in equivalent concentrations of cations is therefore directly reflecting melting temperatures without specifying exactly the nature of dissolved ions. Placing the Ca^{2+} by any other bivalent cation (like Mg^{2+}) would

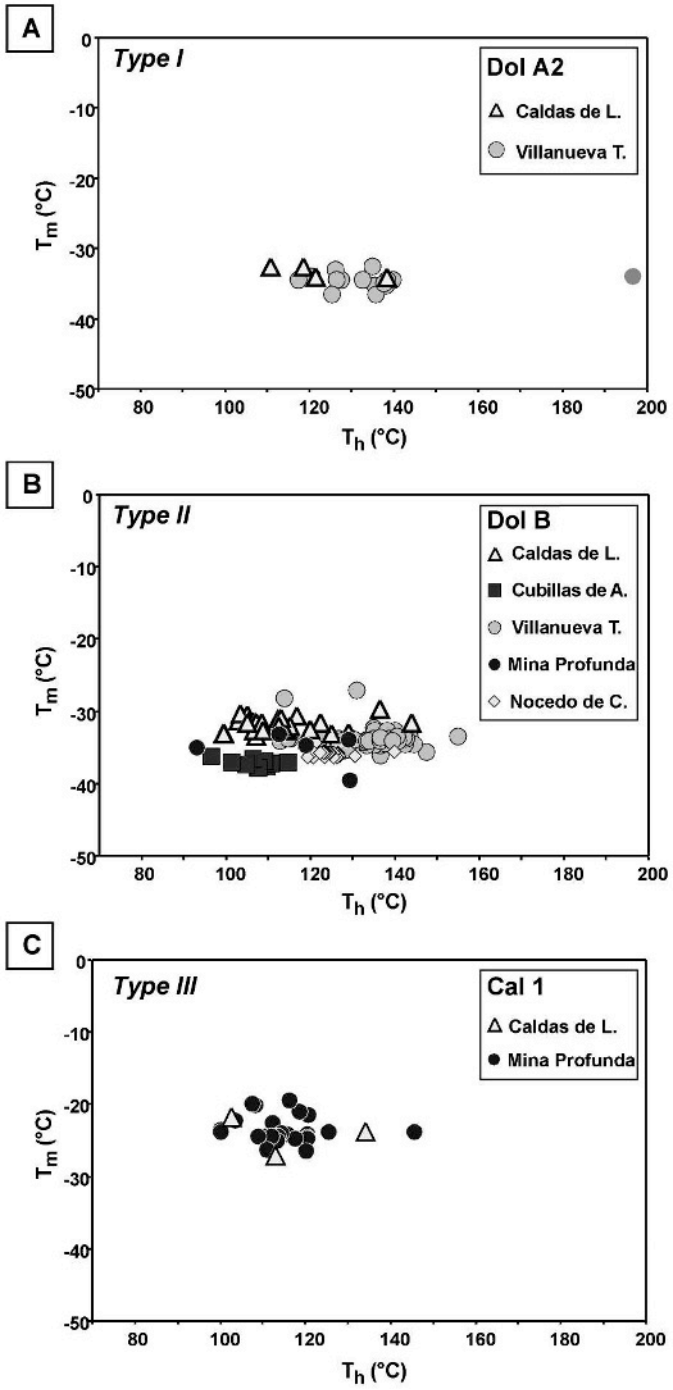

FIG. 10.—Bivariate plots showing the covariance between T_h and T_m values. **A)** *Type I* inclusions in *Dol A2*. **B)** Type II inclusions in *Dol B*. **C)** Type III inclusions in *Cal 1*.

result in similar equivalent mass percentages. Therefore, the obtained variation in equivalent Na^+/Ca^{2+} ratios in *Dol B* is representing a real variation in Na^+/Me^{2+} ratio, where Me^{2+} can by any kind of bivalent metallic cation. Variation of cation content in aqueous solutions can be induced by several mechanisms, such as (1) mixing of two distinct fluids or (2) evolution of one fluid during progressive water–rock interaction. The first process (open system) may have a very irregular distribution pattern in the rock, depending on specific tectonic settings and stratifications. Growth zones in single dolomite crystals could reveal an irregular distribution of specific salinities. The second process (relatively closed system) would cause a regular distribution of distinct salinities in the same growth zones, because the fluid may slowly change its properties during dolomite precipitation. A systematic distribution of different salinities was not observed in *Dol B*. The cryo-Raman spectroscopy method gives the possibility to study variations of this kind, which cannot be deduced from bulk fluid analyses.

Type III inclusions in *Cal 1* are substantially different from the inclusions in *Dol A2* and *Dol B*, inasmuch as they do not reveal a significant variation in cation ratios and only NaCl is identified from salt-hydrate spectra. Minor amounts of other salts such as $CaCl_2$ and $MgCl_2$ could only be suspected from low T_e values.

Dolomite Origin and Calcite Precipitation

Dol A1 and *Dol A2* are two different textural types of the same dolomite phase. The textural differences possibly reflect variability in coarseness and/or impurity content of the precursor carbonate particles, prior to dolomitization (see Gregg and Sibley 1984). This interpretation matches the presence of the *Dol A1–Dol A2* banding exclusively in the lower Barcaliente Fm., where normal grading, reflecting particle size heterogeneity, is the dominant structure. Additionally, *Dol A2* is considered a recrystallization product of *Dol A1*, which may result in similar textures. This implies that its occurrence is independent of the original grading in the precursor carbonatic rock, which is not consistent with the previously mentioned argument.

The textural transition from replacive towards void-filling dolomites occurs gradually and with no reaction boundaries (Fig. 5A). The mother fluids of *Dol A2* and *Dol B* were characterized by similar temperature, density, and salinity as determined from fluid-inclusion investigation. This suggests rather constant physicochemical conditions during the formation of the various dolomite phases. The dolomitization was a continuous process, which evolved from a replacive towards a void-filling stage in a nearly isothermal and isochemical system. The various dolomite phases formed, therefore, from a common hydrothermal and hypersaline brine.

The absence of reaction boundaries between *Cal 1* and *Dol B* suggests that the *Cal 1* mother fluid was dolomite saturated. *Cal 1* possibly precipitated from the same hydrological system of the dolomites, after slight cooling and dilution of the brines. The evolution from *Dol B* towards *Cal 1* precipitation could reflect a shift from the dolomite stability field into the calcite stability field, induced by an increase in the Ca^{2+}/Mg^{2+} ratio and/or a decrease in temperature of the fluid system (see Land 1985; Usdowski 1994). The Ca^{2+}/Mg^{2+} ratio in the fluid in primary inclusions could not be determined. The estimated Na^+/Me^{2+} ratio increased and stabilized at a high level during calcite precipitation, but this ratio does not define calcite/dolomite stability fields.

Cal 2 postdated all of the mineral phases investigated. Reaction boundaries and corroded *Dol B* crystals in contact with *Cal 2* suggest that the calcite precipitated from dolomite-undersaturated fluids. Primary all-liquid inclusions in *Cal 2* (type V) formed at shallow depth, from low-temperature fluids ($< 50°C$), likely of meteoric origin. This suggests that the study area was exposed or near surface at the time of *Cal 2* precipitation, to allow surface fluids to enter the studied rocks.

Reequilibration of Fluid Inclusions

The spread in T_h data reported for types I, II, and III inclusions (Fig. 8) is not likely to be due to stretching by overheating and consequent thermal reequilibration (e.g., Presbindowski and Larese 1987). Inclusions affected by thermal reequilibration commonly have an asymmetric distribution of the T_h data, with most of the values falling into the lower part of the range (e.g., Goldstein and Reynolds 1994). T_h

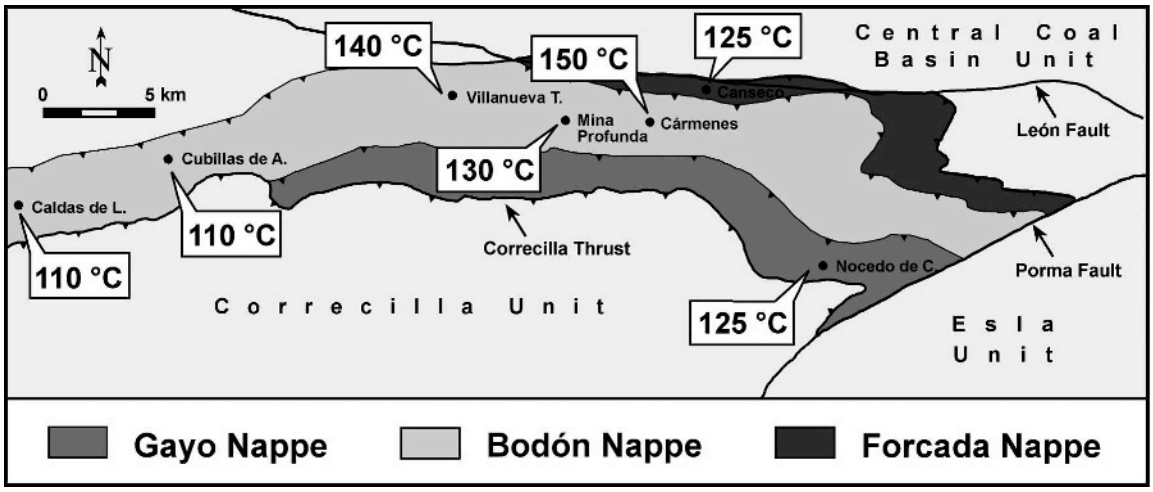

FIG. 11.—Tectonic sketch of the central and eastern Bodón Unit illustrating the sampled sites and the regional variation of the T_h mode values for inclusions in *Dol B* (type II).

for the investigated fluid inclusions approximate either a normal distribution (see Fig. 8) or have an asymmetric distribution, with most of the values falling into the higher part of the range. Therefore, the reported T_h variability is possibly related to temperature fluctuations of circulating fluids or temperature differences between localities. Most likely it reflects slight variations in the crystal growth conditions (including solubility, temperature, and pressure).

Fluid-Trapping Conditions

There is a lack of information on the sedimentation and exhumation history of the study area after the Variscan nappe emplacement. Due to the complex superposition of the nappes, the different areas were affected by differential erosion after Stephanian exposure (e.g., Aramburu and Bastida 1995). Additionally, the scarcity of Stephanian and Permian deposits close to the study area prevents the evaluation of their original thickness. Consequently, the burial depth of the samples at the time of dolomitization cannot be constrained unambiguously. Recent structural balancing of the Southern Cantabrian Basin suggests a minimum tectonically induced overburden of 3.5 km in the area close to the León Fault, on the top of today's erosional level (Veselovsky 2004).

The results of fluid-inclusion investigation were used to estimate the P–T trapping conditions of the various inclusion types along their isochores. The inclusion-trapping conditions were graphically constrained by means of assumed paleo–geothermal gradients. These were constructed using a geothermal gradient of 35°C/km and geobarometric gradients of 10.1 and 27.1 MPa/km for hydrostatic and lithostatic regimes, respectively (Fig. 16). The subsurface temperature was taken at 10°C. Trapping conditions for types I, II, and III inclusions were obtained by the intersection of isochores and geothermal gradients in both hydrostatic and lithostatic regimes. The isochores corresponding to the T_h mode values were used to calculate mean trapping conditions, whereas those corresponding to the maximum and minimum T_h values were used to indicate the variation in possible trapping conditions. Inclusions having anomalous T_h values (i.e., too low or too high relative to the normal distribution of data) were not considered. In a hydrostatic regime, the dolomitization (*Dol A2* and *Dol B*) took place at 150 ± 30°C and 40 ± 10 MPa (Fig. 16), corresponding to a depth of 3.9 ± 1.0 km. In a lithostatic regime, the process took place at 195 ± 40°C and 140 ± 30 MPa (Fig. 16), corresponding to 5.3 ± 1.4 km depth. *Cal 1* precipitated at 130 ± 20°C and 35 ± 5 MPa at slightly higher levels in a hydrostatic regime (3.4 ± 0.6 km depth), and at 170 ± 30°C and 125 ± 20 MPa at slightly higher levels in a lithostatic regime (4.6 ± 0.8 km depth). A hydrostatic geothermal gradient for pore fluids is more likely to be present in these types of rocks, which were affected only by diagenetic temperatures (Brime 1981, 1985; Aller and Brime 1985; Raven and Van der Pluijm 1986; García-López et al. 1997) and thin-skinned tectonics. Moreover, at depths between 3 to 5 km these rocks may have had a relatively high (up to 10%) porosity (e.g., Choquette and James 1990).

TABLE 3.—*Melting temperatures of four* type II *inclusions in* Dol B *cooled following different procedures (i.e. fast cycling and stepwise cycling). The calculated equivalent mass% NaCl and $CaCl_2$ are also reported. Ratio = the fraction NaCl of the sum NaCl + $CaCl_2$.*

					Total salinity (mass %)		
	Inclusion	T_m(X) (°C)	T_m(ice) (°C)	T_m(hydrohalite) (°C)	NaCl	$CaCl_2$	Ratio
Stepwise Cycling	1	−42.5	−22.0	−10.5	24.95	0.44	0.982
	2	−41.3	−22.6	−18.1	23.98	0.87	0.965
	3	−42.8	−33.2	−11.0	6.66	21.90	0.233
	4	−43.3	−29.0	−12.0	8.97	18.27	0.329
Fast Cycling	1		−34.0		—	26.2	
	2		−28.0		—	24.0	
	3		−35.0		—	26.5	
	4		−32.2		—	25.6	

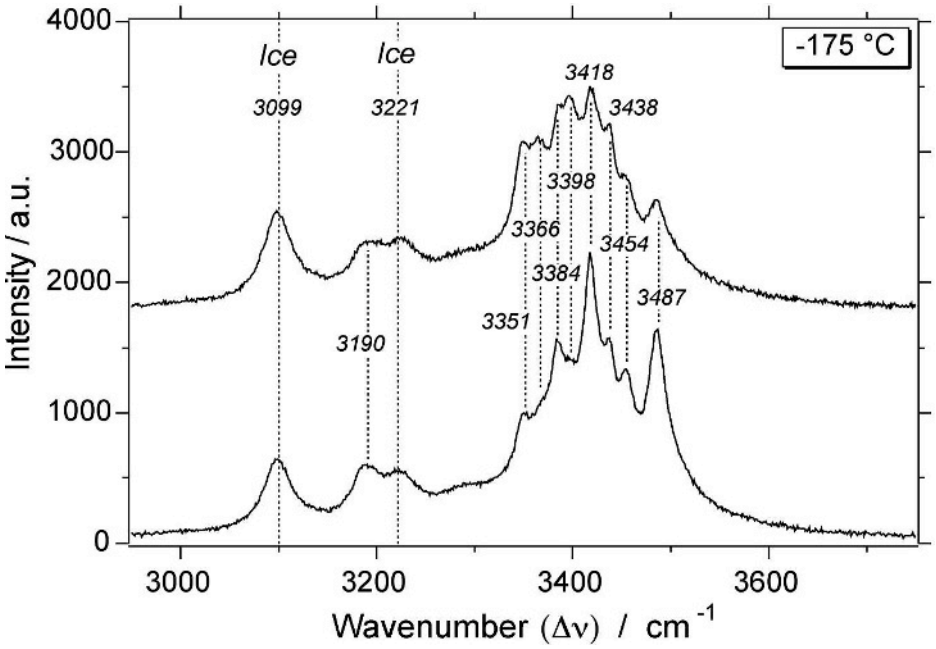

FIG. 12.—Raman spectra showing the different peaks recognized in type II inclusions (*Dol B*) cooled by a stepwise cycling procedure: ice (3009 and 3221 cm^{-1}) and complex salt-hydrate solid solution. Rock sample: VCBD1B, Barcaliente Fm., Villanueva de la Tercia.

Further consideration of the paleo–geothermal gradient in the study area is necessary to better constrain the thermal conditions of the dolomitizing fluids. García-López et al. (1997) and Brime et al. (2001) suggested a gradient of 35°/km for the Bodón Unit at the time of peak burial in the Westphalian. In the Cantabrian Zone a thermal peak occurred in Late Stephanian and especially Early Permian times, when crustal thinning, intense volcanism, and localized magmatism took place (Lepvrier and Martínez-García 1990; Gutiérrez-Alonso et al. 2004). Aller and Brime (1985) invoked a "high geothermal gradient at the transition from Carboniferous to Permian" to explain metamorphism and cleavage in the Central Coal Basin Unit. Frings et al. (2004) proposed a geothermal gradient approaching 85°C/km for a Stephanian basin located south of the study area. This high gradient is thought to be related to Early Permian magmatic activity localized within the Stephanian succession and cannot be extrapolated to areas outside the basin. The timing inferred for the dolomitization (Late Stephanian–Early Permian; Gasparrini 2003; Gasparrini et al. in press) coincides with the occurrence of this thermal peak. Consequently, the geothermal gradient of the study area at the time of dolomitization was likely higher than the gradient of 35°C/km used for calculations. Therefore, the calculated P–T of trapping are the maximum possible for the dolomitizing fluids, whereas the homogenization conditions represent the minimum P–T of trapping. True dolomitization conditions must be somewhere in between.

Regional Variations

The regional distribution of T_h for types I and II inclusions in the Bodón Unit illustrates several trends. The mother fluids of *Dol A2* (type I

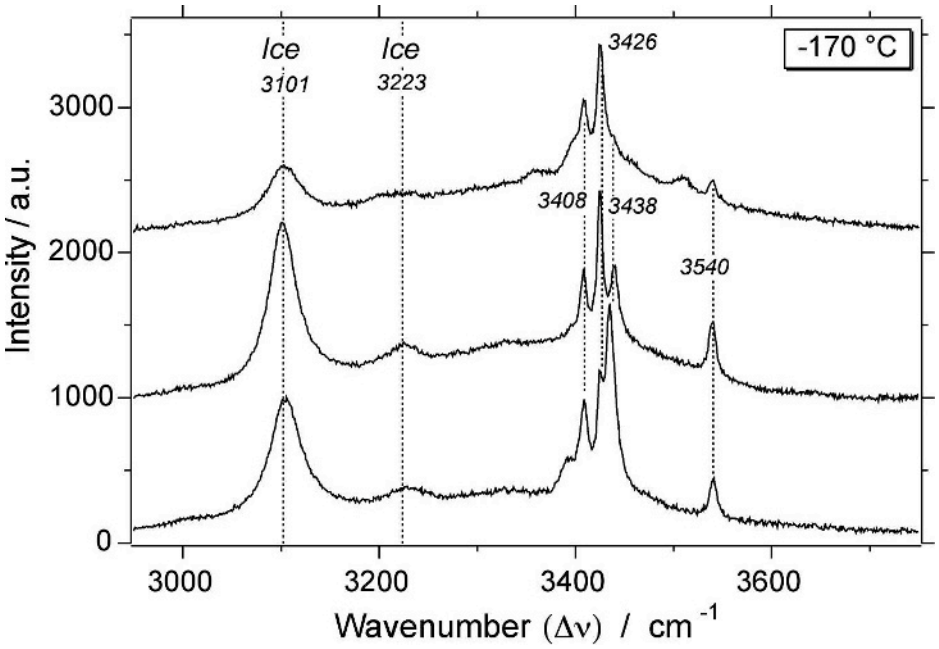

FIG. 13.—Raman spectra showing the different peaks recognized in type II inclusions (*Dol B*) after demixing of the complex salt-hydrate solid solution: ice (3101 and 3223 cm^{-1}) and hydrohalite (3408, 3426, 3438, 3540 cm^{-1}). Rock sample: VCBD1B, Barcaliente Fm., Villanueva de la Tercia.

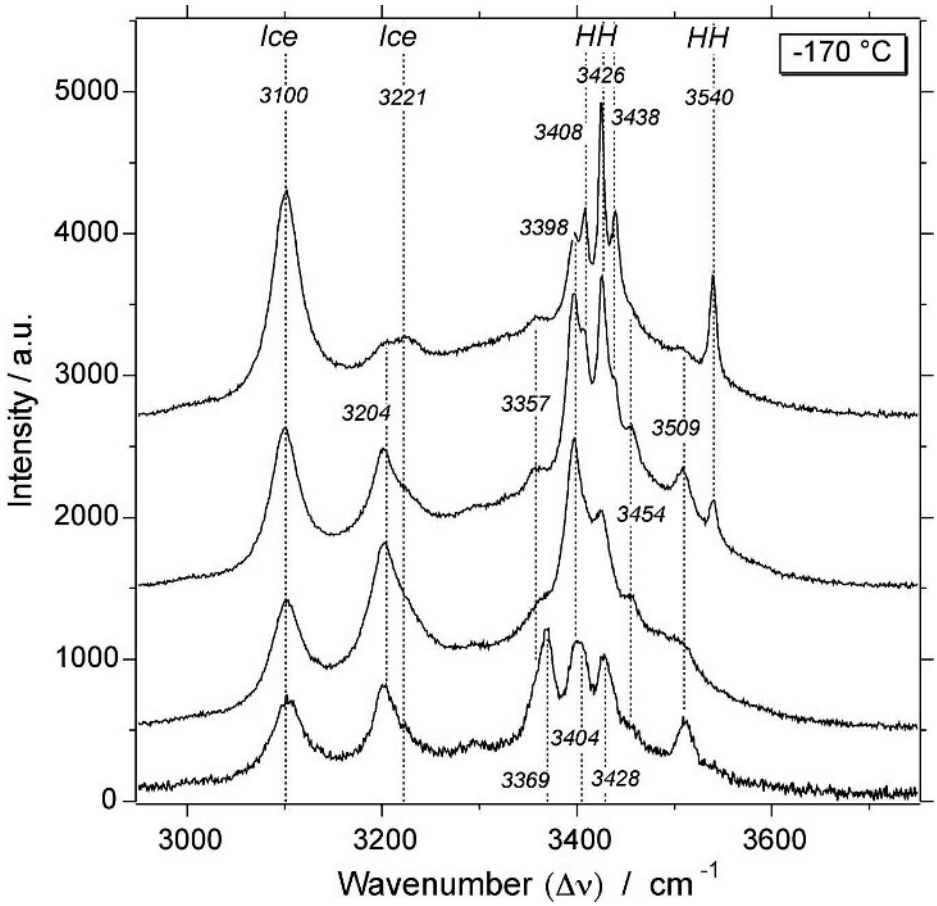

FIG. 14.—Raman spectra showing the different peaks recognized in type II inclusions (*Dol B*) after demixing of the complex salt-hydrate solid solution: ice (3100 and 3221 cm^{-1}), hydrohalite (HH; 3408, 3426, 3438 and 3540 cm^{-1}), and two unknown salt-hydrates (see X and Y in Table 4). Rock sample: VCBD1B, Barcaliente Fm., Villanueva de la Tercia.

inclusions) in the Forcada Nappe display lower T_h values than in the Bodón Nappe. Therefore, the first stage of dolomitization (*Dol A1* and *Dol A2*) possibly occurred at shallower levels in the Forcada Nappe. Type II inclusions (*Dol B*) display the highest T_h values in the center of the Bodón Unit (Cármenes), whereas western (Caldas de Luna) and eastern (Nocedo de Curueño) areas show lower T_h values (Fig. 11). This temperature contour cuts through the individual nappes in the Bodón Unit. An effective hydrothermal cell must have been developed in the center of the Bodón Unit during the growth of *Dol B*. Consequently, large amounts of carbonate rocks were dolomitized at higher temperatures in the center, whereas less pervasive dolomitization occurred in outer sectors and at lower temperatures. In summary, first-stage replacive dolomitization (*Dol A1* and *Dol A2*) is controlled mainly by thrust boundaries and regional tectonic discontinuities such as the León Fault, whereas late-stage void-filling dolomitization (*Dol B*) occurred by means of hydrothermal cells crosscutting thrust boundaries.

TABLE 4.— *Raman shift (peak position in wavenumbers, cm^{-1}) of the different salt-hydrates recognised in* type II *inclusions. X and Y represent two unknown types of salt hydrate. See text for further detail.*

Complex	Hydrohalite	X	Y
3190	3408	3204	3369
3351	3426	3357	3404
3366	3438	3398	3428
3384	3540	3454	
3398		3509	
3418			
3438			
3454			
3487			

CONCLUSIONS

1. A detailed study of fluid inclusions in dolomite, which formed during diagenesis of carbonate rock, supplies a large amount of information about formation conditions, i.e., temperature, depth, and chemistry of dolomitizing systems. The method applied in this study combines microthermometry and Raman spectroscopy to single fluid inclusions and enlarges greatly the analytical accuracy and interpretation possibilities of dolomitizing fluids. It is, therefore, a valuable contribution to the discussion and implications of dolomite research (the "dolomite problem").
2. Five phases of late diagenetic mineral deposition were recognized in massively dolomitized Carboniferous carbonates in the Bodón Unit of the southwestern Cantabrian Zone (NW Spain): two textural types of replacive dolomite (*Dol A1* and *Dol A2*), a void-filling dolomite (*Dol B*), and two types of calcite cements (*Cal 1* and *Cal 2*).
3. Primary, two-phase liquid-rich aqueous inclusions in *Dol A2, Dol B*, and *Cal 1* were investigated by microthermometry only to characterize the dolomitizing fluids. Both *Dol A2* and *Dol B* contain highly saline fluids (23.7 to 29.2 eq. mass % $CaCl_2$) that homogenize at similar temperatures (mode is 130–140°C). *Cal 1* precipitated in chemical equilibrium with the dolomites after minor

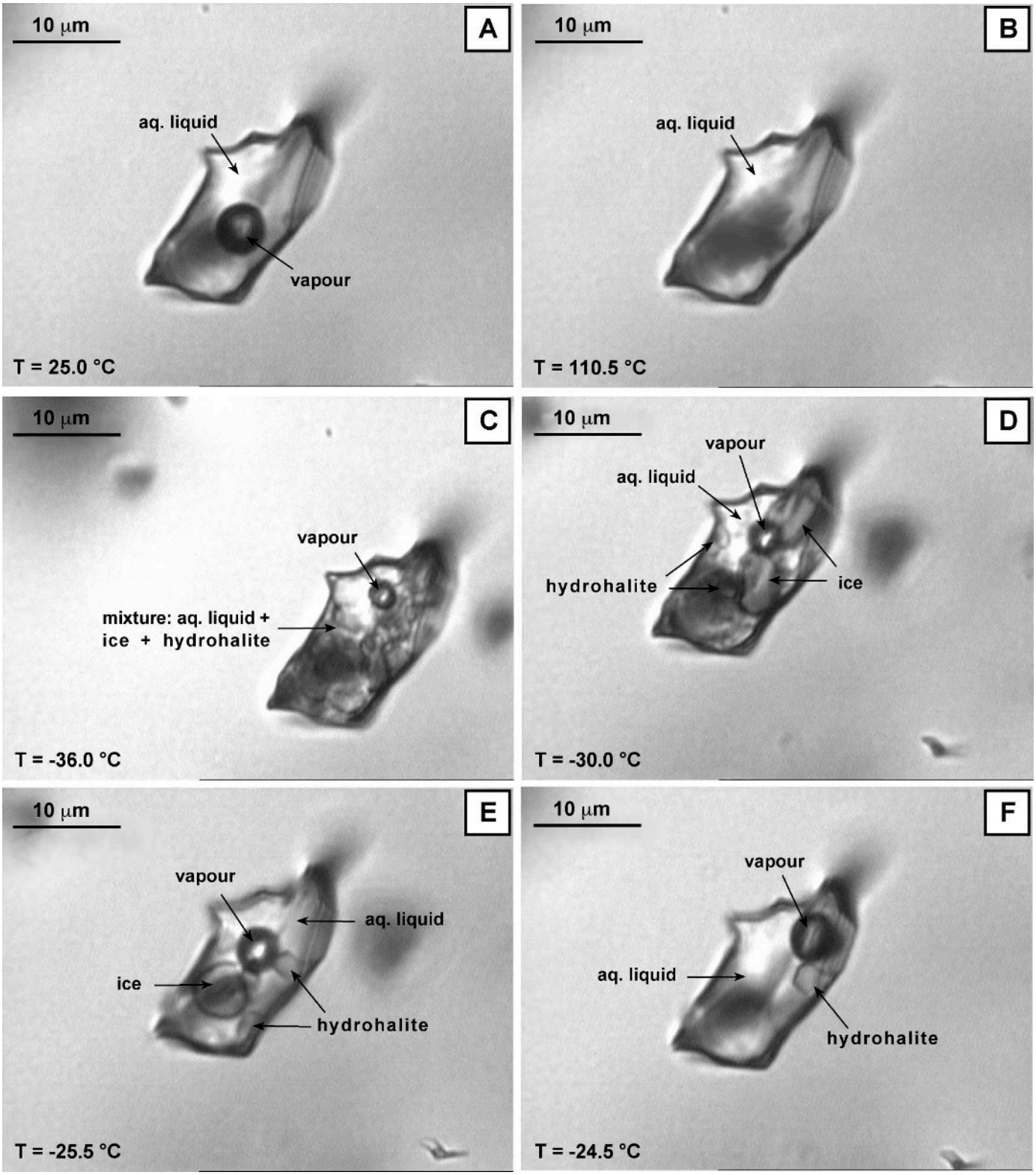

FIG. 15.—Sequence of photographs showing phase changes during a heating–freezing cycle of a type III inclusion (*Cal 1*). Rock sample: MPBD2M, Barcaliente Fm., Mina Profunda. **A)** At room temperature aqueous liquid and a vapor bubble coexisted. **B)** At 110.5°C total homogenization occurred in the liquid phase. **C)** At −36.0°C, after occurrence of the first melting, a mixture of ice, hydrohalite, and aqueous liquid coexisted with a distorted vapor bubble. **D)** At −30.0°C ice, hydrohalite, and aqueous liquid are optically distinguishable. The vapor bubble expanded. **E)** At −25.5°C coarse crystals of ice and hydrohalite coexisted with aqueous liquid and a vapor bubble. **F)** At −24.5°C, after melting of ice, a large hydrohalite crystal coexisted with aqueous liquid and a vapor bubble.

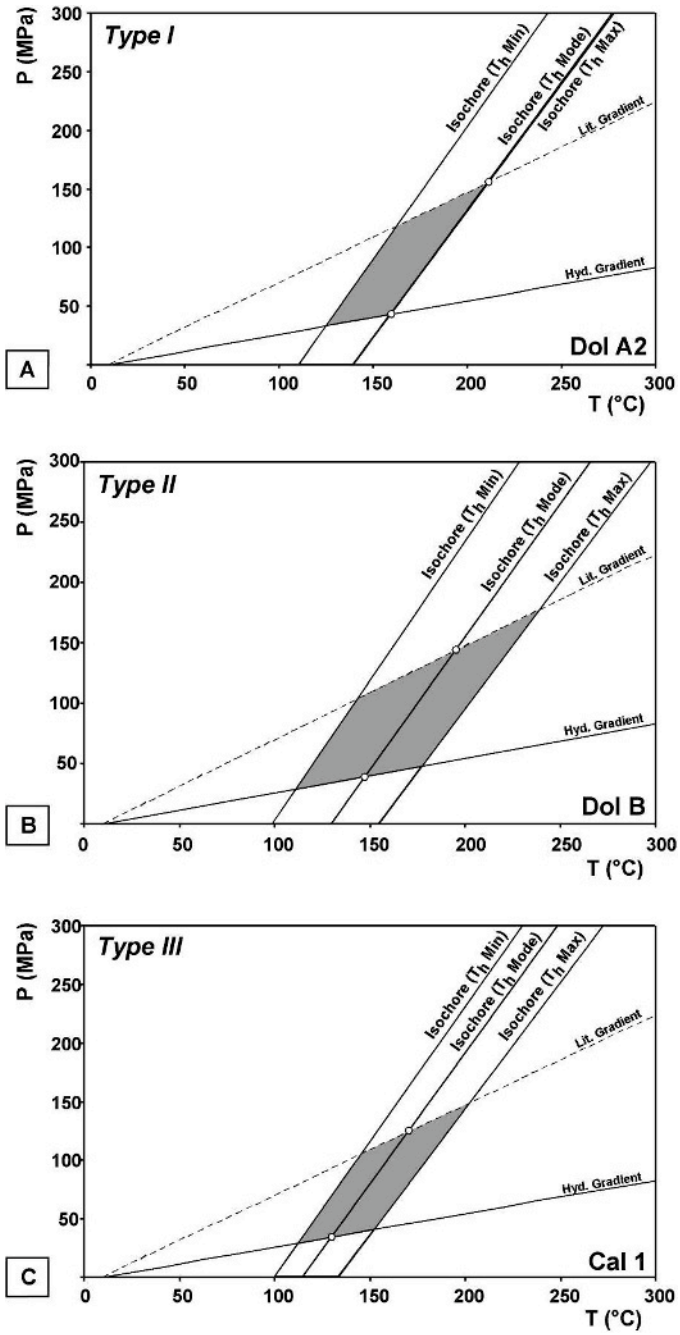

FIG. 16.—P–T plots showing the isochores constructed from the minimum, the mode, and the maximum T_h values and their intersection points with the hydrostatic and lithostatic gradients. **A)** Type I inclusions in *Dol A2*. **B)** Type II inclusions in *Dol B*. **C)** Type III inclusions in *Cal 1*.

cooling (homogenization mode is 115°C) and dilution of the circulating fluids (salinity is 20.3–23.4 eq. mass % $CaCl_2$). *Cal 2* formed from low-temperature (< 50°C), possibly meteorically-derived fluids and marked the near-surface exposure of the study area.

4. Cryo-Raman spectroscopy reveals more detail on the major salt components in individual fluid inclusions and gives more accurate measurements of ice and salt hydrate melting, at eutectics, peritectics, and final melting temperatures. It is illustrated that different cooling procedures may induce the formation of different phase assemblages within the fluid inclusions. Fast cycling experiments inhibited the nucleation of salt hydrates and resulted in a metastable phase assemblage given by ice and a highly saline aqueous liquid. Slow and stepwise cycling experiments resulted in stable phase assemblages of ice and salt hydrates. Consequently, the fluid inclusions displayed different melting behaviors (i.e., different melting temperatures of ice), corresponding to different values of the calculated salinities. Salinity calculation from microthermometry data lead only to an underestimation of the true salinities.
5. Calculated equivalent mass % in the H_2O–NaCl–$CaCl_2$ fluid system obtained from cryo-Raman spectroscopy result in a highly variable equivalent Na/Ca ratio in *Dol B* inclusions. Dolomitization or other water–rock interaction processes may have progressively altered the fluid system, or mixing with external fluids may have changed the cation content of the dolomitizing fluid. This evolving fluid system did not affect the stability of dolomite. In contrast, the approximately constant Na/Ca ratio in *Cal 1* inclusions reflects a regular and homogeneous source for the salts.
6. Cryo-Raman spectroscopy revealed the presence of three types of salt hydrates in *Dol B* inclusions, comprising hydrohalite and two unknown hydrates (one of which resembles $MgCl_2 \cdot 12H_2O$), and only hydrohalite in *Cal 1* inclusions. The presence of $CaCl_2$ hydrates can be suspected only from low eutectic temperatures of inclusions in both *Dol B* (−50 to −57°C) and *Cal 1* (−46 to −50°C).
7. According to a hydrostatic geothermal gradient, maximum formation conditions for the dolomites are at 150 ± 30°C and 40 ± 10 MPa, corresponding to a depth of 3.9 ± 1.0 km. Maximum formation conditions for Cal 1 are at 130 ± 20°C and 35 ± 5 MPa, corresponding to a depth of 3.4 ± 0.6 km. The minimum P–T of formation for these mineral phases are represented by the homogenization conditions of their primary fluid inclusions.
8. Regional variation in homogenization and melting temperatures of fluid inclusions suggests that the replacive dolomitization occurred at shallower levels in the Forcada Nappe than in the Bodón Nappe. The void-filling dolomitization occurred in the center of the Bodón Unit by a hydrothermal cell that effectively crosscut several thrust nappes. Western and eastern parts of the Bodón Unit underwent less intense dolomitization, at slightly lower temperatures.

ACKNOWLEDGMENTS

This work represents part of M. Gasparrini's PhD thesis, funded by the DFG (German Research Foundation), "Graduirtenkolleg" Program 273 on Fluid Rock Interaction, at the Faculty of Geosciences, University of Heidelberg. We wish to thank M. Boni of the Department of Geophysics and Volcanology, University of Naples, for providing suggestions and stimulating discussion on dolomitization. We greatly appreciate D. Banks, C. Brime, A. Csoma, J. Hendry, L. Melim, and B. Yardley for reviewing our manuscript. Appendix 1 has been archived and is available in digital form from the JSR Data Archive, URL: http://www.sepm.org/archive/index.html#JSR.

REFERENCES

ALLER, J., AND BRIME, C., 1985, Deformación y metamorfismo en la parte sur de la Cuenca Carbonífera Central (NO de España): Dixième Congrès International de Stratigraphie et Géologie du Carbonifère, Madrid, Compte Rendu, v. 10, p. 541–548.

ALONSO, J.L., AND PULGAR, J.A., 1995, La estructura de la Zona Cantábrica, *in* Aramburu, C., and Bastida, F., eds., 1995, Geología de Asturias: Gijón, TREA, p. 103–112.

ARAMBURU, C., and BASTIDA, F., eds., 1995, Geología de Asturias: Gijón, TREA, 314 p.

BAKKER, R.J., 2002, Identification of salts in fluid inclusions by combined Raman spectroscopy and low temperature microthermometry, *in* Kontak, D.J., and Anderson, A.J., eds., PACROFI VIII, Pan American Conference on Research on Fluid Inclusions; Halifax, Proceedings, p. 38–42.

Bakker, R.J., 2003, Package FLUIDS 1, Computer programs for analysis of fluid inclusion data and for modelling bulk fluid properties: Chemical Geology, v. 194, p. 3–23.

Bakker, R.J., 2004, Raman spectra of fluid and crystal mixtures in the system H_2O, H_2O–NaCl and H_2O–$MgCl_2$ at low temperatures: applications to fluid inclusion research: The Canadian Mineralogist, v. 42, p. 1283–1314.

Bakker, R.J., and Diamond, L.W., 2006, Estimation of volume fractions of liquid and vapor phases in fluid inclusions, and definition of inclusion shapes: American Mineralogist, v. 91, p. 635–657.

Banks, D.A., and Yardley, B.W.D., 1992, Crush-leach analysis of fluid inclusions in small natural and synthetic samples: Geochimica et Cosmochimica Acta, v. 56, p. 245–248.

Brime, C., 1981, Postdepositional transformation of clays in Paleozoic rocks of northwest Spain: Clay Minerals, v. 16, p. 421–424.

Brime, C., 1985, A diagenesis to metamorphism transition in the Hercynian of NW Spain: Mineralogical Magazine, v. 49, p. 481–484.

Brime, C., García-López, S., Bastida, F., Valín, M.L., Sanz-López, J., and Aller, J., 2001, Transition from diagenesis to metamorphism near the front of the Variscan regional metamorphism (Cantabrian Zone, northwestern Spain): Journal of Geology, v. 109, p. 363–379.

Choquette, P.W., and James, N.P., 1990, Limestones—the burial diagenetic environment, *in* McIlreath, I.A., and Morrow, D.W., eds., Diagenesis: Ottawa, Geoscience Canada, Reprint series, v. 4, p. 75–111.

Coniglio, M., Sherlock, R., Williams-Jones, A.E., Middleton, K., and Frape, S.K., 1994, Burial and hydrothermal diagenesis of Ordovician carbonates from the Michigan Basin, Ontario, Canada, *in* Purser, B.H., Tucker, M.E., and Zenger, D.H., eds., Dolomites—A Volume in Honour of Dolomieu: International Association of Sedimentologists, Special Publication 21, p. 231–254.

Corretgé, L.G., and Suárez, O., 1990, Cantabrian and Palentian Zone: igneous rocks, *in* Dallmeyer, R.D., and Martínez-García, E., eds., Pre-Mesozoic Geology of Iberia: Heidelberg, Springer, p. 72–79.

Dubessy, J., Audeoud, D., Wilkins, R., and Kosztolanyi, C., 1982, The use of the Raman Microprobe Mole in the determination of the electrolytes dissolved in the aqueous phase of fluid inclusions: Chemical Geology, v. 37, p. 137–150.

Fernández-Suárez, J., Dunning, G.R., Jenner, G.A., and Gutiérrez-Alonso, G., 2000, Variscan collisional magmatism and deformation in NW Iberia: constraints from U–Pb geochronology of granitoids: Geological Society of London, Journal, v. 157, p. 565–576.

Frings, K., Lutz, R., De Wall, H., and Warr, L.N., 2004, Coalification history of the Stephanian Ciñera–Matallana pull-apart basin, NW Spain: combining anisotropy of vitrinite reflectance and thermal modelling: International Journal of Earth Sciences, v. 93, p. 92–106.

García-López, S., Brime, C., Bastida, F., and Sarmiento, G.N., 1997, Simultaneous use of thermal indicators to analyse the transition from diagenesis to metamorphism: an example from the Variscan Belt of northwest Spain: Geological Magazine, v. 143, p. 323–334.

Gasparrini, M., 2003. Large-scale hydrothermal dolomitisation in the southwestern Cantabrian Zone (NW Spain): causes and controls of the process and origin of the dolomitising fluids [Ph.D. thesis]: Germany, Ruprecht-Karls-Universität Heidelberg, http://www.ub.uni-heidelberg.de/archiv/3586, 193 p.

Gasparrini, M., Bechstädt, T., and Boni, M., in press, Massive hydrothermal dolomitization in the southwestern Cantabrian Zone (Spain) and its relation to the late Variscan evolution: Marine and Petroleum Geology.

Gleeson, S.A., 2003, Bulk analysis of electrolytes in fluid inclusions, *in* Samson, I., Anderson, A., and Marshall, D., eds., Fluid Inclusions—Analyses and Interpretation: Mineralogical Association of Canada, Short Course 32, p. 233–246.

Goldstein, R.H., and Reynolds, T.J., 1994. Systematics of Fluid Inclusions in Diagenetic Minerals: SEPM, Short Course 31, 198 p.

Gómez-Fernández, F., Both, R.A., Mangas, J., and Arribas, A., 2000, Metallogenesis of Zn–Pb carbonate-hosted mineralization in the southeastern region of the Picos de Europa (central northern Spain) province: geologic, fluid inclusion, and stable isotope studies: Economic Geology, v. 95, p. 19–40.

Gregg, J.M., and Sibley, D.F., 1984, Epigenetic dolomitization and the origin of xenotopic dolomite texture: Journal of Sedimentary Petrology, v. 54, p. 908–931.

Grimmer, J.O.W., 2000. Fluidassoziierte Brekzien als Monitor dolomitisierender und dedolomitisierender Lösungströme in der Kantabrischen Zone (Nordspanien) [Ph.D. thesis]: Germany, Ruprecht-Karls-Universität Heidelberg, http://www.ub.uni-heidelberg.de/archiv/1423, 148 p.

Gutiérrez-Alonso, G., Fernández-Suárez, J., and Weil, A.B., 2004, Orocline triggered lithospheric delamination, *in* Sussman, A.J., and Weil, A.B., eds., Orogenic Curvature: Integrating Paleomagnetic and Structural Analyses: Geological Society of America, Special Paper 383, p. 121–130.

Hemleben, C., and Reuther, C.D., 1980, Allodapic limestones of the Barcaliente Formation (Namurian A) between Luna and Cea rivers (southern Cantabrian Mountains, Spain): Neues Jahrbuch für Geologie und Paleontologie, Abhandlungen, v. 159, p. 225–255.

Krumgalz, B.S., Pogorelsky, R., and Pitzer, K.S., 1996, Volumetric properties of single aqueous electrolytes from zero to saturation concentrations at 298, 15 K represented by Pitzer's Ion-Interaction Equation: Journal of Physical Chemistry Reference Data, v. 25, p. 663–689.

Land, L.S., 1985, The origin of massive dolomite: Journal of Geological Education, v. 33, p. 112–125.

Lepvrier, C., and Martínez-García, E., 1990, Fault development and stress evolution of the post-Hercynian Asturian Basin (Asturias and Cantabria, NW Spain): Tectonophysics, v. 184, p. 345–356.

Machel, H.G., 2005, Concepts and models of dolomitization: a critical reappraisal, *in* Braithwaite, C.J.R., Rizzi, G., and Darke, G., eds., The Geometry and Petrogenesis of Dolomite Hydrocarbon Reservoirs: Geological Society of London, Special Publication 235, p. 7–63.

Marcos, A., 1968a, La tectonica de la Unidad de la Sobia–Bodón: Trabajos de Geología, v. 2, p. 59–87.

Marcos, A., 1968b, Nota sobre el significado da la "Leon Line:" Breviora Geologica Asturica, v. 3, p. 1–5.

Marcos, A., Kullmann, J., and Schönenberg, R., 1979, Facies differentiation caused by wrench deformation along a deep-seated fault system (León Line, Cantabrian Mountains, North Spain)—Discussion and Reply: Tectonophysics, v. 60, p. 303–309.

McKenzie, J.A., 1991, The dolomite problem: an outstanding controversy, *in* Müller, D.W., McKenzie, J.A., and Weissert, H., eds., Controversies in Modern Geology: London, Academic Press, p. 37–54.

Mernagh, T.P., and Wilde, A.R., 1989, The use of the laser Raman microprobe for the determination of salinity in fluid inclusions: Geochimica et Cosmochimica Acta, v. 53, p. 765–771.

Morrow, D.W., 1990a, Dolomite—Part 1: the chemistry of dolomitization and dolomite precipitation, *in* McIlreath, I.A., and Morrow, D.W., eds., Diagenesis: Ottawa, Geoscience Canada Reprint series, v. 4, p. 113–124.

Morrow, D.W., 1990b, Dolomite—Part 2: dolomitization models and ancient dolostones, *in* McIlreath, I.A., and Morrow, D.W., eds., Diagenesis: Ottawa, Geoscience Canada Reprint Series, v. 4, p. 125–139.

Morrow, D.W., Cumming, G.L., and Aulstead, K.L., 1990, The gas-bearing Devonian Manetoe Facies, Yukon and Northwest Territories: Geological Survey of Canada, Bulletin, v. 400, 54 p.

Naden, J., 1996, CalcicBrine: a Microsoft Excel 5.0 Add-in for calculating salinities from microthermometric data in the system NaCl–$CaCl_2$–H_2O, *in* Brown, P.E., and Hagemann, S.G., eds., PACROFI VI, Pan American Conference on Research on Fluid Inclusion: Madison, Proceedings, p. 97–98.

Nielsen, P., Swennen, R., Muchez, P., and Keppens, E., 1998, Origin of Dinantian zebra-dolomites south of the Brabant–Wales Massif, Belgium: Sedimentology, v. 45, p. 727–743.

Paniagua, A., 1993. Mineralizaciones asociadas a estructuras tardihercínicas en la rama Sur de la Zona Cantábrica [Unpublished Ph.D. thesis]: University of Oviedo, Spain, 377 p.

Paniagua, A., Fontboté, L., Fenoll Hach-Alí, P., Fallick, A.E., Moreiras, D.B., and Corretgé, L.G., 1993, Tectonic setting, mineralogical characteristics, geochemical signatures and age dating of a new type of epithermal carbonate-hosted, precious metal-five element deposits: the Villamanín area (Cantabrian Zone, northern Spain), *in* Fenoll Hach-Alí, P., Torres-Ruiz, J., and Gervilla, F., eds., Current Research in Geology Applied to Ore Deposits: Granada, 2nd biennial Society for Geology Applied to Mineral Deposits (SGA) Meeting, p. 531–534.

Paniagua, A., Rodríguez-Pevida, L.S., Loredo, J., Fontboté, L., and Fenoll Hach-Ali, P., 1996, Un yacimiento de Au en carbonatos del Orógeno Hercínico: el área de Salamón (N León): Geogaceta, v. 20, p. 1605–1608.

Pérez-Estaún, A., and Bastida, F., 1990, Cantabrian Zone: Structure, *in* Dallmeyer, R.D., and Martínez-García, E., eds., Pre-Mesozoic Geology of Iberia: Heidelberg, Springer, p. 55–69.

Presbindowski, D.R., and Larese, R.E., 1987, Experimental stretching of fluid inclusions in calcite—implications for diagenetic studies: Geology, v. 15, p. 333–336.

Radke, B.M., and Mathis, R.L., 1980, On the formation and occurrence of saddle dolomite: Journal of Sedimentary Petrology, v. 50, p. 1149–1168.

Raven, J.G.M., and Van der Pluijm, B.A., 1986, Metamorphic fluids and transtension in the Cantabrian Mountains of northern Spain: an application of the conodont colour alteration index: Geological Magazine, v. 123, p. 673–681.

Reuther, C.D., 1980, The Lower Carboniferous facies levelling and the first Upper Carboniferous tectonic events in the Cantabrian Mountains and the Pyrenees (Spain)—a comparison, *in* Kullmann, J., Schönenberg, R., and Wiedmann, J., eds., Subsidenz-Entwicklung im Kantabrischen Variszikum und an passiven Kontinental-raendern der Kreide: Tübingen, Neues Jahrbuch für Geologie und Palaontologie, p. 244–250.

Roedder, E., 1984, Fluid Inclusions: Mineralogical Society of America, Reviews in Mineralogy, v. 12, 644 p.

Samson, I.M., and Walker, R.T., 2000, Cryogenic Raman Spectroscopy studies in the system NaCl–$CaCl_2$–H_2O: The Canadian Mineralogist, v. 38, p. 35–43.

Sibley, D.F., and Gregg, J.M., 1987, Classification of dolomite rock textures: Journal of Sedimentary Geology, v. 57, p. 967–975.

Spötl, C., and Pitman, J.K., 1998, Saddle (baroque) dolomite in carbonates and sandstones: a reappraisal of a burial-diagenetic concept, *in* Morad, S., ed., Carbonate Cementation in Sandstones: International Association of Sedimentologists, Special Publication 26, p. 437–460.

Tornos, F., and Spiro, B.F., 2000, The geology and isotope geochemistry of the talc deposits of Puebla de Lillo (Cantabrian Zone, northern Spain): Economic Geology, v. 95, p. 1277–1296.

Usdowski, E., 1994, Synthesis of dolomite and geochemical implications, *in* Purser, B.H., Tucker, M.E., and Zenger, D.H., eds., Dolomites—A Volume in Honour of Dolomieu: International Association of Sedimentologists, Special Publication 21, p. 345–360.

VESELOVSKY, Z., 2004, Integrated numerical modelling of a polyhistory basin, Southern Cantabrian Basin (Palaeozoic, NW-Spain): Gaea Heidelbergensis [CD-ROM], v. 13, 225 p.

WAGNER, R.H., WINKLER PRINS, C.F., AND RIDING, R.E., 1971, Lithostratigraphic units of the lower part of the Carboniferous in northern León, Spain: Trabajos de Geología, v. 4, p. 603–663.

WALLACE, M.W., BOTH, R.A., MORALES RUANO, S., HACH-ALI, P.F., AND LEES, T., 1994, Zebra textures from carbonate-hosted sulfide deposits: sheet cavity networks produced by fracture and solution enlargement: Economic Geology, v. 89, p. 1183–1191.

WILKINSON, J.J., 2003, On diagenesis, dolomitisation and mineralisation in the Irish Zn–Pb orefield: Mineralium Deposita, v. 38, p. 968–983.

WILSON, E.N., LAWRENCE, A.H., AND PHILLIPS, O.M., 1990, Dolomitization front geometry, fluid flow patterns, and the origin of massive dolomite: the Triassic Latemar buildup, northern Italy: American Journal of Science, v. 290, p. 741–796.

WOJCIK, K.M., GOLDSTEIN, R.H., AND WALTON, A.W., 1994, History of diagenetic fluids in a distant foreland area, Middle and Upper Pennsylvanian, Cherokee basin, Kansas, USA: Fluid inclusion evidence: Geochimica et Cosmochimica Acta, v. 58, p. 1175–1191.

ZHANG, Y.J., AND FRANTZ, J.D., 1987, Determination of the homogenisation temperatures and densities of supercritical fluids in the system NaCl–KCl–$CaCl_2$–H_2O using sythetic fluid inclusions: Chemical Geology, v. 64, p. 335–350.

Received 6 October 2005; accepted 20 April 2006.

UNITED STATES POSTAL SERVICE™

Statement of Ownership, Management, and Circulation
(Required by 39 USC 3685)

	2. Publication Number	3. Filing Date
Journal of Sedimentary Research	1 5 2 7 - 1 4 0 4	
4. Issue Frequency: Six times a year	5. Number of Issues Published Annually: 6	6. Annual Subscription Price: $350.00

7. Complete Mailing Address of Known Office of Publication (Not printer) (Street, city, county, state, and ZIP+4): Society for Sedimentary Geology, 6128 E 38th St, Suite #308, Tulsa OK 74135-5814
Contact Person: Michele Woods
Telephone: 800-865-9765

8. Complete Mailing Address of Headquarters or General Business Office of Publisher (Not printer): Society for Sedimentary Geology, 6128 E 38th St, Suite #308, Tulsa OK 74135-5814

9. Full names and Complete Mailing Addresses of Publisher, Editor, and Managing Editor (Do not leave blank)
Publisher (Name and complete mailing address): Society for Sedimentary Geology, 6128 E 38th St, Suite #308, Tulsa OK 74135-5814
Editor (Name and complete mailing address): Kitty L. Milliken and Colin P. North, Journal of Sedimentary Research, Department of Geological Sciences, University of Colorado, 399 UCB, Boulder CO 80309-0399
Managing Editor (Name and complete mailing address): Melissa Lester, Journal of Sedimentary Research, Department of Geological Sciences, University of Colorado, 399 UCB, Boulder CO 80309-0399

10. Owner (Do not leave blank. If the publication is owned by a corporation, give the name and address of the corporation immediately followed by the names and addresses of all stockholders owning or holding 1 percent or more of the total amount of stock. If not owned by a corporation, give the names and addresses of the individual owners. If owned by a partnership or other unincorporated firm, give its name and address as well as those of each individual owner. If the publication is published by a nonprofit organization, give its name and address.)

Full Name	Complete Mailing Address
Society for Sedimentary Geology	6128 E 38th St, Suite #308, Tulsa OK 74135-5814

11. Known Bondholders, Mortgagees, and Other Security Holders Owning or Holding 1 Percent or More of Total Amount of Bonds, Mortgages, or Other Securities. If none, check box → ☑ None

Full Name	Complete Mailing Address

12. Tax Status (For completion by nonprofit organizations authorized to mail at special rates) (Check one)
The purpose, function, and nonprofit status of this organization and the exempt status for federal income tax purposes:
☑ Has Not Changed During Preceding 12 Months
☐ Has Changed During Preceding 12 Months (Publisher must submit explanation of change with this statement)

PS Form 3526, September 1998 (See Instructions on Reverse) Computerized Facsimile

13. Publication Title: Journal of Sedimentary Research			14. Issue Date for Circulation Data Below: September-06	
15. Extent and Nature of Circulation			Average No. Copies Each Issue During Preceding 12 Months	Actual No. Copies of Single Issue Published Nearest to Filing Date
a. Total Number of Copies *(Net press run)*			2633	1800
b. Paid and/or Requested Circulation	(1)	Paid/Requested Outside- County Mail Subscriptions stated on Form 3541. *(Include advertiser's proof and exchange copies)*	1400	1038
	(2)	Paid In-County Subscriptions *(Include advertiser's proof and exchange copies)*	0	0
	(3)	Sales Through Dealers and Carriers, Street Vendors, Counter Sales, and Other Non-USPS Paid Distribution	4	4
	(4)	Other Classes Mailed Through the USPS	886	833
c. Total Paid and/or Requested Circulation *(Sum of 15b(1), (2),(3), and (4))* ▶			2290	1875
d. Free Distribution by Mail Samples,complimentary, and other free)	(1)	Outside-County as Stated on Form 3541	0	0
	(2)	In-County as Stated on Form 3541	0	0
	(3)	Other Classes Mailed Through the USPS	0	0
e. Free Distribution Outside the Mail *(Carriers or other means)*			4	4
f. Total Free Distribution *(Sum of 15d and 15e)* ▶			4	4
g. Total Distribution *(Sum of 15c and 15f)* ▶			2294	1879
h. Copies not Distributed			340	121
i. Total (Sum of 15g. and h.) ▶			2633	1800
j. Percent Paid and/or Requested Circulation (15c divided by 15g times 100)			99.8	99.8

16. Publication of Statement of Ownership
☐ Publication required. Will be printed in the _____ issue of this publication. ☐ Publication not required.

17. Signature and Title of Editor, Publisher, Business Manager, or Owner: Hunter L. Scott, Assoc. Director + Business Mgr. Date: 10-1-06

I certify that all information furnished on this form is true and complete. I understand that anyone who furnishes false or misleading information on this form who omits material or information requested on the form may be subject to criminal sanctions (including fines and imprisonment) and/or civil sanctions (including civil penalties).

Instructions to Publishers

Complete and file one copy of this form with your postmaster annually on or before October 1. Keep a copy of the completed form for your records.
In Cases where the stockholder or security holder is a trustee, include in items 10 and 11 the name of the person or corporation for whom the trustee is acting. Also include the names and addresses of individuals who are stockholders who own or hold 1 percent or more of the total amount of bonds, mortgages, or other securities of the publishing corporation. In item 11, if none, check the box. Use blank sheets if more space is required.
Be sure to furnish all circulation information called for in item 15. Free circulation must be shown in items 15d, e, and f.
Item 15h., Copies not Distributed, must include (1) newsstand copies originally stated on Form 3541, and returned to the publisher, (2) estimated returns from news agents, and (3), copies for office use, leftovers, spoiled, and all other copies not distributed.
If the publication had Periodicals authorization as a general or requester publication, this Statement of Ownership, Management, and Circulation must be published; it must be printed in any issue in October or, if the publication is not published during October, the first issue printed after October.
In item 16, indicate the date of the issue in which this Statement of Ownership will be published.
Item 17 must be signed.

Failure to file or publish a statement of ownership may lead to suspension of second-class authorization.

Form 3526, September 1998(Reverse) Computerized Facsimile